Check for updates

JGR Atmospheres

RESEARCH ARTICLE
10.1029/2024JD042733

Special Collection:
Recent progress in atmospheric boundary layer turbulence and implications to surface-atmosphere exchange

Turbulence of Tropical Cyclones: From Peristrophic to Zonostrophic

Boris Galperin[1], Alexander K. Nickerson[1], Gregory P. King[2], and Jun A. Zhang[3,4]

[1]College of Marine Science, University of South Florida, St. Petersburg, FL, USA, [2]Independent Scholar, ATTIC Research Associates, Selkirk, UK, [3]Hurricane Research Division, Atlantic Oceanographic and Meteorological Laboratory, National Oceanic and Atmospheric Administration, Miami, FL, USA, [4]Cooperative Institute for Marine and Atmospheric Studies, University of Miami, Miami, FL, USA

Key Points:

- Cyclostrophic turbulence in the inner region of tropical cyclones (TCs) is decoupled from its ambient counterpart
- With increasing storm intensity, the cyclostrophic turbulence evolves from peristrophic to zonostrophic
- The eyewall of a TC is an equivalent of an eastward zonal jet on giant planets

Correspondence to:
J. A. Zhang,
jun.zhang@noaa.gov

Citation:
Galperin, B., Nickerson, A. K., King, G. P., & Zhang, J. A. (2025). Turbulence of tropical cyclones: From peristrophic to zonostrophic. *Journal of Geophysical Research: Atmospheres*, *130*, e2024JD042733. https://doi.org/10.1029/2024JD042733

Received 17 OCT 2024
Accepted 30 JUN 2025

Author Contributions:
Conceptualization: Boris Galperin, Alexander K. Nickerson, Gregory P. King
Data curation: Alexander K. Nickerson
Formal analysis: Alexander K. Nickerson
Funding acquisition: Jun A. Zhang
Investigation: Alexander K. Nickerson, Gregory P. King, Jun A. Zhang
Methodology: Boris Galperin, Alexander K. Nickerson, Gregory P. King, Jun A. Zhang
Project administration: Jun A. Zhang
Resources: Boris Galperin, Gregory P. King
Software: Boris Galperin, Alexander K. Nickerson
Supervision: Boris Galperin, Gregory P. King, Jun A. Zhang
Validation: Alexander K. Nickerson, Gregory P. King, Jun A. Zhang

© 2025. The Author(s).
This is an open access article under the terms of the Creative Commons Attribution License, which permits use, distribution and reproduction in any medium, provided the original work is properly cited.

Abstract Cyclostrophic rotation in the core region of tropical cyclones (TCs) imprints a distinct signature upon their turbulence structure. Its intensity is characterized by the radius of maximum wind, R_{mw}, and the azimuthal wind velocity at that radius, U_{max}. The corresponding cyclostrophic Coriolis parameter, $\hat{f} = 2U_{max}/R_{mw}$, far exceeds its planetary counterpart, f, for all storms; its impact increases with storm intensity. The vortex can be thought of as a system undergoing a superposition of planetary and cyclostrophic rotations represented by the effective Coriolis parameter, $\tilde{f} = \hat{f} + f$. On the vortex periphery, $\tilde{f}$ merges with f. In the classical Rankine vortex model, the inner region undergoes solid-body rotation rendering $\hat{f}$ constant. In a more realistic representation, $\hat{f}$ is not constant, and the ensuing cyclostrophic β-effect sustains vortex Rossby waves. Horizontal turbulence in such a system can be quantified by a two-dimensional anisotropic spectrum. An alternative description is provided by one-dimensional, longitudinal, and transverse spectra computed along the radial direction. For rotating turbulence with vortex Rossby waves, the spectra divulge a coexistence of three ranges: Kolmogorov, peristrophic (spectral amplitudes are proportional to $\tilde{f}^2$), and zonostrophic (transverse spectrum amplitude is proportional to $\hat{\beta}^2$). A comprehensive database of TC winds collected by reconnaissance airplanes reveals that with increasing storm intensity, their cyclostrophic turbulence evolves from purely peristrophic to mixed peristrophic-zonostrophic to predominantly zonostrophic. The latter is akin to the flow regime harboring zonal jets on fast rotating giant planets. The eyewall of TCs is an equivalent of an eastward zonal jet.

Plain Language Summary Data from hundreds of reconnaissance flights into Atlantic and Pacific storm systems demonstrate that with increasing central pressure drop, their turbulence becomes increasingly anisotropic. Hurricanes of categories 4 and 5 attain a flow regime known as zonostrophic turbulence. The same regime governs the appearance of zonal (east-west) jets and coherent vortices visible from spacecraft and telescopes on fast-rotating giant planets. Moreover, the eyewall of tropical cyclones is an equivalent of an eastward zonal jet on giant planets.

1. Introduction

The extensive volume of literature on the dynamics of tropical cyclones (TCs) devotes surprisingly little attention to their turbulence structure. Only a few studies consider the role of turbulence in important dynamical processes such as TC formation and maintenance, see for example, Schecter (2011), Emanuel et al. (2023), and Oguejiofor et al. (2024), or attaining observed intensity (Bryan et al., 2010; Bryan & Rotunno, 2009a, 2009b). Renewed interest in TC turbulence has been inspired by the analysis of recent reconnaissance aircraft observations by Zhang (2010), Tang et al. (2015), Byrne and Zhang (2013), Vonich and Hakim (2018), Prasanth et al. (2020), and numerical simulations by Wang et al. (2018), Zheng et al. (2020), and Yu et al. (2022) as well as by the studies of the effect of turbulence on storm predictability by Rotunno and Snyder (2008), Judt et al. (2016), and Kieu and Rotunno (2022). Byrne and Zhang (2013) found that the direction of energy transfer may change with altitude, whereas Tang et al. (2015) observed a similar phenomenon in the horizontal. Vonich and Hakim (2018) documented affinity between the kinetic energy (KE) spectra obtained from reconnaissance observations and those established for tropospheric and lower stratospheric turbulence in the Global Atmospheric Sampling Program (GASP) (Nastrom et al., 1984; Nastrom & Gage, 1985). The GASP spectra will be denoted NG85 henceforward. Likewise, a similarity was noticed between the results obtained from the MOZAIC campaign (Marenco et al., 1998) and the meiyu front system (Peng et al., 2014). The observational tropospheric spectra are comprised

21698996, 2025, 14, Downloaded from https://agupubs.onlinelibrary.wiley.com/doi/10.1029/2024JD042733, Wiley Online Library on [24/08/2025]. See the Terms and Conditions (https://onlinelibrary.wiley.com/terms-and-conditions) on Wiley Online Library for rules of use; OA articles are governed by the applicable Creative Commons License

Writing – original draft: Boris Galperin, Alexander K. Nickerson
Writing – review & editing: Boris Galperin, Gregory P. King, Jun A. Zhang

of two branches, one of which exhibits, approximately, the Kolmogorov $-5/3$ slope in the subsynoptic range of scales, and the other one approaches the power law exponent -3 in the synoptic range. One needs to be careful with the interpretation of observations, however, because these two independent branches can produce nearly any slope between $-5/3$ and -3 contingent upon their concatenation point. The same is true not only for atmospheric and oceanic flows, see, for example, Thompson (1973), Trenberth and Solomon (1993), Kurgansky (2008), Bierdel et al. (2016), and Biri et al. (2016), but also for turbulence in other environments, such as the solar photosphere (Chaouche et al., 2020).

Vonich and Hakim (2018) found that although the TC spectra for every category on the Saffir-Simpson scale appear nearly isomorphic to their NG85 counterparts, the amplitudes of the former monotonically rise with storm intensity. The TC slopes became steeper across horizontal scales from 10 to 160 km, and their steepest slopes increased from -1.9 to -3.1 while evolving from tropical depression to category 5. Mirroring this steepening, the transition zone between the mild and steep slopes shifted downscale with increasing category.

The affinity of the TC and NG85 spectra is intriguing yet the physics behind it is poorly understood. An important point to keep in mind is that the original NG85 papers dealt only with zonal and meridional *longitudinal* spectra averaged around the latitude of 30°N. Vonich and Hakim (2018), on the other hand, investigated radial spectra of the azimuthal velocity, that is, the *transverse* TC spectra. Their comparison of the TC and NG85 spectra should be taken with caution because the one-dimensional (1D) longitudinal and transverse spectra are different not only in rotating flows but even in flows with no rotation at all as explained by Sukoriansky and Galperin (2016) and Galperin and Sukoriansky (2020).

Sukoriansky and Galperin (2016) investigated turbulence with rotation in the framework of the quasi-normal scale elimination (QNSE) theory. This theory is a modification of the renormalization group theory of turbulence (RNG; Yakhot & Orszag, 1986). The Navier-Stokes equations in this theory are mapped onto the stochastically forced Langevin equations. The forcing is assumed quasi-normal. Using this approach, the governing equations undergo successive coarse-graining that yields scale-dependent renormalized viscosities and diffusivities. Sukoriansky and Galperin (2016) adapted this theory to a rotating coordinate frame. Along with anisotropic eddy viscosities and eddy diffusivities, they derived analytical expressions for longitudinal and transverse KE spectra. The spectra exhibit a bi-modal structure predicated by a superposition of the Kolmogorov (spectral exponent $\sim k_1^{-5/3}$) and Coriolis (spectral exponent $\sim k_1^{-3}$) branches on small and large scales. In these exponents, k_1 is the magnitude of a 1D wave vector. Since the Coriolis branch includes the factor f^2 (f is the Coriolis parameter, $f = 2\Omega \sin\phi$, where Ω and ϕ are the angular velocity of Earth's rotation and the latitude, respectively), we hereby designate this spectrum as *peristrophic*. This term originates from the Greek word *περιστροφή* reading *peristrophy* and meaning *rotation*. The rotation can be of any nature, either weak or strong.

With the parameters specific to the GASP and MOZAIC campaigns, the theoretical QNSE spectra were found to accurately represent those obtained in observations (Galperin & Sukoriansky, 2020). Given the mentioned earlier similarity of the NG85 and TC spectra and keeping in mind that rotational effects dominate both phenomena, one can ponder whether or not the QNSE theory applies to the TC turbulence and is capable of explaining and quantifying the spectra observed by Vonich and Hakim (2018).

Attributing TC spectra to the peristrophic regime summons an immediate conundrum: tropical storms populate latitudes around 20°N, hence their Coriolis parameter is approximately constant. Spectral amplitudes of TCs, however, monotonically increase with rising storm intensity.

To decipher this puzzle and account for the dependence of spectral amplitudes on the strength of system rotation, we bring into consideration a cyclostrophic Coriolis parameter, $\hat{f}$, formally introduced later in Section 2. This parameter is related to the intensity of storm rotation in the assumption that the inner core of the vortex features solid-body rotation, that is, $\hat{f} = const$. We shall see that by adding $\hat{f}$ to f, as stipulated by the superposition of two collinear inertial forces, the observed rise of spectral amplitudes with storm intensity can be partially explained and quantified by the QNSE theory.

Various data sets indicate that with increasing category, the TC spectral slopes may become steeper than -3. As an example, Vonich and Hakim (2018) demonstrated that with the increase of turbulence intensity in the vicinity of TC eyewall, the transverse spectrum can attain a slope of -3.1 for category 5 storms. Steep spectral slopes were also reported in simulations by Prasanth et al. (2020). In addition, numerical experiments by Kieu and

21698996, 2025, 14, Downloaded from https://agupubs.onlinelibrary.wiley.com/doi/10.1029/2024JD042733, Wiley Online Library on [24/08/2025]. See the Terms and Conditions (https://onlinelibrary.wiley.com/terms-and-conditions) on Wiley Online Library for rules of use; OA articles are governed by the applicable Creative Commons License

Rotunno (2022) exposed significant disparity between the radial and azimuthal spectra in strong storms. The peristrophic framework and the Rankine vortex model are insufficient to explain these findings.

The peristrophic regime is not the only one that can develop in turbulence with rotation. A small deviation of f from a constant value with, approximately, a linear rate β produces a β-effect that evokes Rossby waves. The interaction of these waves with turbulence leads to spectral anisotropization, steepening of the slopes, and formation of a unique circulation regime harboring alternating zonal jets. This regime, known as *zonostrophic turbulence*, has been detected in experiments, computer simulations, and on fast-rotating giant planets. These results have been summarized in Chapter 13 of a book by Galperin and Read (2019). Following up experiments by Lemasquerier et al. (2023) confirmed most of the preceding findings. Cabanes et al. (2024) detected the zonostrophic regime in simulations of subsurface oceans on Jovian satellites. Sukoriansky et al. (2008, 2012) and Cohen et al. (2024) found that along with the zonal jets, flows in the zonostrophic regime contain coherent vortices, denoted zonons, interspersed between and traveling with the jets. Most of the vortices and vortex trains on both Jupiter and Saturn can be associated with the zonons.

An approximately linear deviation from the solid-body rotation in the TC cores, measured by a cyclostrophic β, denoted $\hat{\beta}$, produces a cyclostrophic β-effect that supports the *vortex Rossby waves* discussed by for example, Macdonald (1968), Yamagata (1976), Carr and Williams (1989), Montgomery and Kallenbach (1997), McWilliams et al. (2003), and Zaqarashvili et al. (2021). Wang and Wu (2004) refer to them as "Rossby-type waves in circular vortex."

One can ponder whether or not a regime similar to zonostrophic turbulence may develop in a TC vortex. If the answer is assertive, then the next question is whether or not a combined effect of $\hat{f}$ and $\hat{\beta}$ can cause TC turbulence to acquire both peristrophic and zonostrophic properties. Although one cannot rule out the coexistence of these regimes, the currently available planetary data point to the prevalence of the latter on Jupiter (Galperin et al., 2014). A strong β-effect and available data resolution limit our ability to explore other regimes on Jupiter and Saturn at the present time. Planetary data are also insufficient for a detailed spectral analysis as of yet. However, TC vortices span a wide range of cyclostrophic rotation in which the intensity of a β-effect changes from relatively weak in tropospheric flows to very strong in category 5 storms. Thus, tropical storms offer an attractive natural laboratory for investigations of various rotational regimes as well as their interactions and transitions. The results of these studies are at the focus of the present study.

The narration continues with Section 2 that provides theoretical background and delineates various flow regimes, whereas Section 3 compares the results of this analysis with theoretical predictions. Section 4 furthers the analysis and summarizes conclusions. Details of our data set and data analysis are given in Appendix A.

2. A Model of TC Turbulence

In analogy with other studies, for example, Adem and Lezama (1960), Macdonald (1968), Anthes and Hoke (1975), Chan and Williams (1987), Carr and Williams (1989), Fiorino and Elsberry (1989), Shapiro and Ooyama (1990), Carr and Elsberry (1997), Montgomery and Kallenbach (1997), Möller and Montgomery (1999), Nolan and Montgomery (2000), McWilliams et al. (2003), Kuo et al. (2008), and Martinez et al. (2022), the investigation of storm vortices will be conducted in a barotropic framework and in a steady-state, as in, for example, Malkus and Riehl (1960) and Emanuel (1995). Although this is an idealized approach, it will allow us to concentrate on the intricacies of the effect of rotation on turbulence. Observations (Vonich & Hakim, 2018) and simulations (Kieu & Rotunno, 2022) indicate that at aircraft flight levels, hurricane winds are nearly entirely azimuthal. We note the different nature of the tropospheric and TC rotation. The former is maintained by rotation of Earth and characterized by the NG85 spectra. The latter is cyclostrophic and maintained by convection and the central pressure drop (Holton, 2004). With r and $U(r)$ being the radius and the azimuthal wind velocity, respectively, the cyclostrophic angular velocity is $\hat{\Omega}(r) = U(r)/r$ and the cyclostrophic Coriolis parameter is $\hat{f}(r) = 2\hat{\Omega}(r)$. The cyclostrophic velocity attains its maximum, U_{max}, at the radius of maximum wind, $r = R_{mw}$, that is, $U_{max} = U(R_{mw})$.

The values of the basic TC parameters used in this study are summarized in Table 1 as functions of the storm intensity traditionally measured in terms of the Saffir-Simpson scale. The latter is well correlated with the mean drop in sea level pressure denoted ΔP_{SL} measured between the center of TC and 500 km radius. The values of ΔP_{SL} in the present study agree well with other estimates, such as those by Chavas et al. (2017).

21698996, 2025, 14, Downloaded from https://agupubs.onlinelibrary.wiley.com/doi/10.1029/2024JD042733, Wiley Online Library on [24/08/2025]. See the Terms and Conditions (https://onlinelibrary.wiley.com/terms-and-conditions) on Wiley Online Library for rules of use; OA articles are governed by the applicable Creative Commons License

Table 1
Characteristic Storm and Coriolis Parameters Estimated From Mission and Radial Leg Data Per Storm Category

Storm category	$R_{mw}(km)$	$U_{max}(ms^{-1})$	$\Delta P_{SL}(hPa)$	$\phi(°N)$	$f \times 10^5(s^{-1})$	$\hat{f} \times 10^5(s^{-1})$	$\tilde{f} \times 10^5(s^{-1})$	$\hat{\beta} \times 10^9(m^{-1}s^{-1})$
TD	86	11.1	0.1	22.2	5.5	25.8	31.3	3.0
TS	82	20.0	7.1	23.3	5.8	49.0	54.7	6.0
1	64	31.6	24.3	24.9	6.1	99.5	105.7	15.7
2	57	41.2	48.0	26.0	6.4	145.3	151.6	25.6
3	41	47.7	50.3	23.7	5.9	234.7	240.6	57.8
4	28	56.2	65.5	21.2	5.3	401.1	406.3	143.0
5	25	66.2	83.4	19.9	5.0	523.3	528.3	206.8

Note. TD and TS denote Tropical Depression and Tropical Storm, respectively. The symbols have the following meaning: R_{mw}—the radius of maximum wind; U_{max}—maximum wind speed; ΔP_{SL}—sea level pressure difference between 0 and 500 km; ϕ—mean storm latitude; $f, \hat{f}, \tilde{f}$—the planetary, cyclostrophic, and effective Coriolis parameters, respectively; $\hat{\beta}$—cyclostrophic beta.

To the zeroth order, nearly azimuthal TC winds can be represented by the classical Rankine vortex model described by, for example, Ooyama (1982), Carr and Williams (1989), Acheson (1990), Möller and Montgomery (1999), and Stern et al. (2015). In this model, the fluid in the domain $r \le R_{mw}$ is in solid-body rotation and, thus, $\hat{\Omega}(r) = U_{max}/R_{mw} = \hat{\Omega}_0$ and $\hat{f} = 2\hat{\Omega}_0$ are constant.

A TC vortex is subject to a superposition of planetary and cyclostrophic rotations whose local vectors are collinear. To reflect this fact, one can invoke the Principle of Least Action (Landau & Lifshitz, 1976) and represent the compound TC rotation by an *effective* Coriolis parameter,

$$\tilde{f} = f + \hat{f}. \tag{1}$$

A similar representation could, of course, be derived using the Navier-Stokes equation in a rotating coordinate frame, as they both emanate from the same Principle. However, Equation 1 yields a more convenient formulation of a compound rotation in a Cartesian coordinate system used in Equations 4 and 5 below. Furthermore, these equations are consistent with airplane observations taken along straight flight legs, whereas 2D data in such observations are unavailable.

One can relate $\tilde{f}$ to the absolute angular momentum of a TC vortex, $M(r)$, using a general balance equation, for example, Smith et al. (2009),

$$M(r) = U(r)r + \frac{1}{2}r^2 f = \frac{1}{2}r^2\left[\hat{f}(r) + f\right] = \frac{1}{2}r^2\tilde{f}(r). \tag{2}$$

According to Table 1, $\hat{f} \gg f$ for storms of all categories. Neglecting f in Equation 2 yields

$$M(R_{mw}) \equiv M \simeq U_{max}R_{mw}. \tag{3}$$

This equation will be used later.

A TC model based upon Equation 1 with a constant $\hat{f}$ in its core is a generalization of the classical Rankine vortex model. The solid-body rotation facilitates the regime of homogeneous turbulence for $r \le R_{mw}$ and, thus, the applicability of the QNSE expressions for the longitudinal, $E_L(k_1)$, and transverse, $E_T(k_1)$, spectra derived by Sukoriansky and Galperin (2016) with f replaced by $\tilde{f}$,

$$E_L(k_1) = C_L\Pi_\varepsilon^{2/3}k_1^{-5/3} + C_{f1}\tilde{f}^2k_1^{-3}, \tag{4}$$

$$E_T(k_1) = C_T\Pi_\varepsilon^{2/3}k_1^{-5/3} + C_{f2}\tilde{f}^2k_1^{-3}. \tag{5}$$

21698996, 2025, 14, Downloaded from https://agupubs.onlinelibrary.wiley.com/doi/10.1029/2024JD042733, Wiley Online Library on [24/08/2025]. See the Terms and Conditions (https://onlinelibrary.wiley.com/terms-and-conditions) on Wiley Online Library for rules of use; OA articles are governed by the applicable Creative Commons License

Here, $C_L \simeq 0.49$, $C_T \simeq 0.65$, and the two basic model constants for the Coriolis range are $C_{f1} = 0.0926$ and $C_{f2} = 0.24$. As explained by, for example, Golitsyn (2018), Π_ε in these equations denotes the horizontal energy flux. These equations were derived for the case of downscale energy transfer, that is, $\Pi_\varepsilon > 0$. However, there exist indications that the transfer direction and so the sign of Π_ε may change, possibly, discontinuously (Sahoo et al., 2017), although the spectra preserve their Kolmogorov-like shape (Boffetta, 2023; Byrne & Zhang, 2013; Pouquet et al., 2017). The uncertainty in the sign of Π_ε degrades to some extent the accuracy of its determination if estimated by curve fitting to theoretical expressions. This is a consequence of the dependence of C_L and C_T on the direction of the energy transfer.

Upon exit from the TC vortex, in the limit $\tilde{f} \to f$, the predicted spectra Equations 4 and 5 are expected to merge with those of the peristrophic regime prevalent in the troposphere. For TC vortices, we shall use the values of ϕ and Π_ε employed by Galperin and Sukoriansky (2020), $\phi = 25°\text{N}$ and $\Pi_\varepsilon = 4 \times 10^{-5}\ \text{m}^2\text{s}^{-3}$.

In more realistic TC models (Carr & Williams, 1989; Riehl, 1963), $\hat{\Omega}$ is allowed to deviate from $\hat{\Omega}_0$ at, approximately, a constant rate $\hat{\beta}$ (Montgomery & Kallenbach, 1997). This parameter, designated as the cyclostrophic β in analogy to the planetary β (Galperin & Read, 2019), is a measure of the radial vorticity gradient (Guimond et al., 2020) that can be estimated as $\hat{\beta} = \hat{f}/R_{mw}$. Cyclostrophic β generates vortex Rossby waves that interact with TC turbulence and render it anisotropic.

From Table 1, we infer that not only $f/\hat{f} \ll 1$ but also $\beta/\hat{\beta} \ll 1$ such that the effects of the cyclostrophic and planetary rotation in TC cores are practically decoupled for storms of all categories. In the vicinity of TC periphery, however, the effects of f and β take over and play significant roles in TC dynamics and movement (Carr & Elsberry, 1997; Franklin et al., 1996).

The cyclostrophic β-effect and the vortex Rossby waves ubiquitous in the data, for example, Corbosiero et al. (2006) and Prasanth et al. (2020), cannot be accommodated within the peristrophic regime, and so this framework needs to be expanded. Given the scantness of theoretical studies analyzing turbulence with Rossby waves and difficulties of incorporating strong anisotropy in analytical theories (Frederiksen & O'Kane, 2023, 2024), this expansion will be guided by the information gleaned from the fusion of data from numerical simulations, laboratory experiments, and planetary observations (Cabanes et al., 2024; Cohen et al., 2024; Galperin & Read, 2019; Lemasquerier et al., 2023; Read, 2024).

Recall that simulations of 2D turbulence on a β-plane in the Cartesian coordinates detailed by Chekhlov et al. (1996) revealed a strongly anisotropic flow dominated by alternating jets in the direction of the axis Ok_1. The Coriolis parameter varied with the constant rate β along the axis Ok_2 orthogonal to Ok_1. The phase speed of the Rossby waves along Ok_2 is zero. The 2D KE spectrum of the β-plane turbulence is strongly anisotropic with the exponent -5 along Ok_2 and Kolmogorov law exponent $-5/3$ in all other directions. Although the 1D spectra were not computed, the longitudinal, $E_L(k_2)$, and transverse, $E_T(k_2)$, spectra of zonal flows on relatively large scales would be expected to be proportional to $\Pi_\varepsilon^{2/3} k_2^{-5/3}$ and $\beta^2 k_2^{-5}$, respectively. For brevity, these spectra have been termed residual and zonal. This taxonomy will be preserved for spectra in other geometries.

These results were scrutinized by Huang et al. (2001) in subsequent simulations of turbulence on the surface of a rotating sphere. As on a β-plane, the flow was highly anisotropic and divulged a system of alternating zonal jets. In the spherical harmonics decomposition, one can define *zonal modes* for which the zonal index, m, is zero. These modes are wave-less as they feature zero Rossby wave frequency and zero meridional phase speed. Thus, the modes represent zonal flows and are akin to annular modes. In real flows, the annular modes are affected by a variety of wave processes and exhibit large meridional undulations that regulate weather and climate (Gerber & Thompson, 2017; Monahan & Fyfe, 2008). On giant planets, zonal jets are corrugated by eddies, eddy trains, and zonons (Cohen et al., 2024). Recent studies by Battalio and Lora (2021) highlighted the importance of annular modes not only for Earth but also for other planets and satellites. In analogy to turbulence on a β-plane, anisotropic energy transfer to zonal modes leads to energy condensation and steepening of their meridional spectrum to the power law proportional to $\beta^2 n^{-5}$ with n being the *total* index. This spectrum corresponds to zonal flows and has been termed *zonal spectrum*. Modes with zonal index $m \neq 0$ form the *residual spectrum*; it obeys the Kolmogorov scaling. The flow regime featuring zonal jets and strongly anisotropic spectrum has been termed *zonostrophic turbulence* (Galperin et al., 2006, 2019).

21698996, 2025, 14, Downloaded from https://agupubs.onlinelibrary.wiley.com/doi/10.1029/2024JD042733, Wiley Online Library on [24/08/2025]. See the Terms and Conditions (https://onlinelibrary.wiley.com/terms-and-conditions) on Wiley Online Library for rules of use; OA articles are governed by the applicable Creative Commons License

To reconcile the results of simulations on a rotating sphere with those on a β-plane, we assume that the Cartesian representation of the residual and zonal spectra via their respective longitudinal and transverse counterparts can be written as

$$E_L(k_1) = C_{KL}\Pi_\varepsilon^{2/3}k_1^{-5/3}, \tag{6}$$

$$E_T(k_1) = C_{KT}\Pi_\varepsilon^{2/3}k_1^{-5/3} + C_Z\beta^2k_1^{-5}, \tag{7}$$

where k_1 is aligned in the direction normal to the zonal flow, that is, along the meridians. Note that Ok_1 is a direction of the zero Rossby wave phase speed. With this orientation of the coordinate axes, the above equations represent the regime of zonostrophic turbulence on a rotating sphere in terms of the 1D spectra in Cartesian coordinates.

The simulations performed by Huang et al. (2001) were purely 2D and so the constants C_{KL} and C_{KT} in Equations 6 and 7 relate to the inverse energy cascade with the rate Π_ε in 2D turbulence. These constants are computed by integrating the isotropic velocity spectrum tensor given by Equation 6.193 in Pope (2018) in 2D plane,

$$C_{KL} = C_{2DK}\frac{\Gamma\left(\frac{5}{6}\right)}{2\pi^{1/2}\Gamma\left(\frac{7}{3}\right)} \simeq 1.6, \tag{8}$$

$$C_{KT} = \frac{5}{3}C_{KL} \simeq 2.7, \tag{9}$$

where $C_{2DK} \simeq 6$ is the Kolmogorov constant for 2D turbulence (Boffetta & Ecke, 2012; Boffetta et al., 2000; Maltrud & Vallis, 1991). The constant C_Z in Equation 7 is $O(1)$.

We need to keep in mind that real flows are 3D and, as elucidated in Section 3.7, the natural flows attaining the regime of zonostrophic turbulence are also 3D. Therefore, in practical applications of Equations 6 and 7, one has to use the constants C_L and C_K appearing in Equations 4 and 5 instead of C_{KL} and C_{KT}.

Goncharov and Pavlov (2004) referred to the modes with zero Rossby wave frequency as the null-modes and noted that they play a special role in the Hamiltonian dynamics of a variety of systems featuring a β-effect or its equivalent. However, they did not consider the interaction of these modes with turbulence.

It is provoking to think that the regime of zonostrophic turbulence can also materialize in TC vortices where vortex Rossby waves are omnipresent. To represent Equations 6 and 7 in cylindrical geometry, we align the axis Ok_1 with the radius. With n being the azimuthal wave number in the notations of Montgomery and Kallenbach (1997), the *zonal vortex modes* correspond to those with $n = 0$. These modes feature a zero vortex Rossby wave frequency and zero radial vortex Rossby wave phase speed. They are similar to zonal flows on a sphere and can be designated as *vortex zonal modes*. In some situations, they may play an important role in the formation and maintenance of *annular hurricanes* (Knaff et al., 2003, 2008) that are akin to annular modes. Regarding spectral representation, in a vortex-centered cylindrical coordinate system (r,θ), the azimuthal and radial spectra can be associated with their longitudinal and transverse counterparts in Cartesian geometry. These spectra are directly measurable in reconnaissance missions described in the next Section. The central quest that we are set to explore is whether or not a vortex system can develop a regime of *vortex zonostrophic turbulence.*

In analogy to zonostrophic turbulence on a β-plane, its vortex version would imply that the interaction of the vortex Rossby waves with turbulence leads to funneling the horizontal energy flux into the vortex zonal mode and formation of a *vortex zonostrophic spectrum* with the power law $\sim\hat{\beta}^2k_1^{-5}$. Here, the planetary β is neglected because $\beta/\hat{\beta} \ll 1$.

Different scaling laws for the longitudinal and transverse spectra are essential properties of the zonostrophic regime. Consequently, to identify this regime from the data in a TC vortex, we shall consider both spectra.

So far, we dealt with idealized 2D flows even though all geophysical and planetary flows are necessarily 3D. Although the two-dimensionalization of atmospheric and oceanic flows under the actions of rotation and stable stratification is a widely accepted paradigm, the inertial waves would be impossible in geophysical flows if they

21698996, 2025, 14, Downloaded from https://agupubs.onlinelibrary.wiley.com/doi/10.1029/2024JD042733, Wiley Online Library on [24/08/2025]. See the Terms and Conditions (https://onlinelibrary.wiley.com/terms-and-conditions) on Wiley Online Library for rules of use; OA articles are governed by the applicable Creative Commons License

were strictly 2D and so, they need to be reckoned with. To accomplish this, we need to move away from Charney's paradigm of geostrophic turbulence (Charney, 1971). This move poses immediate questions: can the peristrophic and zonostrophic regimes coexist, interact, and if so, how?

The wide ranges of $\hat{f}$ and $\hat{\beta}$ available in TCs allow for answering these questions. At the same time, one needs to keep in mind that the derivation of the equations describing the peristrophic regime within the QNSE theory relies upon the assumption of the constant Coriolis parameter that is violated with the presence of a cyclostrophic β-effect. With the understanding that the proposed below model is an approximation, we combine the equations describing the peristrophic and zonostrophic regimes and compare the resulting expressions for the spectra with those observed for different storm intensities.

The hypothetical composite spectra are

$$E_L(k_1) = C_L \Pi_\varepsilon^{2/3} k_1^{-5/3} + C_{fL} \tilde{f}^2 k_1^{-3}, \tag{10}$$

$$E_T(k_1) = C_T \Pi_\varepsilon^{2/3} k_1^{-5/3} + C_{fT} \tilde{f}^2 k_1^{-3} + C_Z \hat{\beta}^2 k_1^{-5}. \tag{11}$$

As mentioned earlier, these spectra are proposed here for the first time, and one of the challenges of the present study is to ascertain their presence in the data collected in TCs of various intensity. It will be shown later that these spectra do exist. They reveal important aspects of TC's dynamics:

1. Turbulence in TCs is strongly anisotropic as divulged by 1D spectra;
2. TC turbulence in the eyewall region approaches the zonostrophic regime;
3. In the inner core, the zonostrophic subrange encroaches into the peristrophic one until the latter is fully expunged.

To quantify these phenomena, we need to introduce several characteristic length scales. The ratio of the eddy turnover timescale, $\tau_{to} = \left(\Pi_\varepsilon k_1^2\right)^{-1/3}$, and the peristrophic timescale, $\tau_p = \tilde{f}^{-1}$, defines a length scale, known as the Woods scale (Sukoriansky & Galperin, 2016), that separates the Kolmogorov and peristrophic subranges,

$$L_\Omega = \left(\Pi_\varepsilon / \tilde{f}^3\right)^{1/2}. \tag{12}$$

Note that for the TC vortices, Equation 12 involves $\tilde{f}$ rather than f. Scales of the order of L_Ω are characterized by the inception of the inverse energy transfer manifesting by a change of sign of Π_ε from positive to negative. The length of the flight legs used to compute the Kolmogorov spectra from aircraft observations described in the next Section is usually larger than L_Ω and so the estimated values of Π_ε include contributions from positive and negative addends. There is no possibility to evaluate each of them separately and so we have to accept that the values of Π_ε are accurate within, probably, an $O(1)$ factor. The sign of Π_ε cannot be determined from the even statistical moments such as spectra but it is immaterial for this study and so it will be presumed positive. The values of C_L and C_T in Equations 10 and 11 will be assumed the same as those in Equations 4 and 5.

Byrne and Zhang (2013) attributed the change in the energy transfer direction to the transitions between 3D and 2D turbulence. Although this is a possible scenario, another alternative is the development of the dual energy cascade due to rotation, see for example, Pouquet et al. (2017). The QNSE theory also supports the change in the energy transfer direction on scales $O(L_\Omega)$ (Sukoriansky & Galperin, 2016).

In a fashion similar to the derivation of Equation 12, the ratio of τ_{to} and the zonostrophic timescale, $\tau_z = \hat{\beta}^{-1} k_1$, defines the transitional scale (Sukoriansky et al., 2007),

$$L_\beta = \left(\Pi_\varepsilon / \hat{\beta}^3\right)^{1/5}, \tag{13}$$

that identifies the transition between the Kolmogorov and zonostrophic subranges and marks the threshold of spectral anisotropization. As we only consider a β-effect in the inner core of a TC vortex where $\hat{\beta} \gg \beta$, the planetary β has been neglected in Equation 13. The estimate of L_β is needed to evaluate the interval between the

21698996, 2025, 14, Downloaded from https://agupubs.onlinelibrary.wiley.com/doi/10.1029/2024JD042733, Wiley Online Library on [24/08/2025]. See the Terms and Conditions (https://onlinelibrary.wiley.com/terms-and-conditions) on Wiley Online Library for rules of use; OA articles are governed by the applicable Creative Commons License

Kolmogorov and zonostrophic subranges and verify that they do not run into each other. Note that the scales from the interval between L_Ω and L_β encompass the peristrophic subrange.

Equation 11 features the superposition of three independent branches with slopes varying between $-5/3$ and -5. Depending on their concatenation points, these branches can accommodate nearly any slope in between, and so the slopes on their own are not very informative. As emphasized earlier in the case of a purely peristrophic regime, the fidelity of agreement between a theory model with data should be judged not by the shape of spectral slopes but by the accuracy of replication of spectral amplitudes. In the case at hand, the amplitudes are known only in the purely peristrophic limit $\tilde{f} \to f$ and the purely zonostrophic limit $\tilde{f} \to 0$. It is unknown a priori whether or not the coefficients C_{fL}, C_{fT}, and C_Z are invariant when all three regimes coexist. Since the above equations cannot be derived analytically at the present time, the interdependence of the coefficients will be assessed from the data. It is important that by their very construction, Equations 10 and 11 asymptotically converge to their respective NG85 counterparts in the limit $\tilde{f} \to f$ at the TC vortex periphery.

3. Comparison of Observations and Theory

3.1. Observations

A data set used in this study was created from about 3,000 reconnaissance aircraft missions into 320 tropical systems (tropical storms and cyclones) in the North Atlantic and eastern Pacific Oceans for the years 1977–2022. The data set included NOAA Best Track (NBT) and Hurricane Research Division (HRD) storm parameters and track information. For more detail, see Appendix A.

Of the 14,650 total flight legs in our database, there are four ranges of flight altitudes that included more than 1,000 flight legs each. In order from most to fewest flight numbers, these ranges are: (a) 3,000–3,500 m, (b) 1,500–2,000 m, (c) 2,500–3,000 m, and (d) 2,000–2,500 m.

The flight patterns from each mission were parsed and trimmed to obtain *radial legs*. Only legs with lengths greater than 10 km and that passed within 25 km of the storm center were used. Individual flight legs were classified according to the maximum storm intensity estimated from the linearly interpolated NBT maximum 60 s sustained wind speed; categories were then assigned according to the Saffir-Simpson scale.

3.2. Storm Parameters, TC Regions, and Scales

Each mission was processed to obtain estimates of the storm latitude, ϕ, and the difference in sea level pressure between the center of the storm and 500 km farther away, ΔP_{SL}. Their averages per category are listed in Table 1.

Data from each radial leg were processed to calculate its specific U_{max} and R_{mw}. These were averaged per category to obtain the mean values listed in Table 1. Also given in the table are the planetary Coriolis parameter, f, the cyclostrophic Coriolis parameter, $\hat{f}$, the effective Coriolis parameter, $\tilde{f}$, Equation 1, and the cyclostrophic beta, $\hat{\beta}$. Recall that $\hat{f}$ and $\hat{\beta}$ are functions of U_{max} and R_{mw}.

Figure 1 shows the dependence of the storm parameters on the mean intensity of the storm. Figures 1a and 1b show that as ΔP_{SL} and U_{max} increase, R_{mw} decreases. The contraction of R_{mw} with increasing storm intensity is consistent with field observations and numerical studies except for hurricanes undergoing rapid intensification (Martinez et al., 2022; Shen, 2006).

The absolute angular momentum of TCs at $r = R_{mw}$ at the tropospheric level is approximated by $M = R_{mw}U_{max}$, Equation 2, and is shown in Figure 1c. Ignoring the value for TD, M varies around a mean of about $17 \times 10^5 \mathrm{m^2 s^{-1}}$ consistent with a recent analysis by Vinour et al. (2021) based on satellite observations. Assuming that the deviations about the mean can be considered small, M is approximately conserved. The conservation of M is behind the compaction of the TC core during the intensification stage. Chavas et al. (2015) mention the inflowing boundary layer air among the physical mechanisms that contribute to the near-conservation of M at low levels.

An insightful analysis of various turbulence regimes and of the horizontal KE flux, Π_ε, requires subdivision of the vortex areas to the inner core region (IR) and the outer region (OR). The IR extends to about $2R_{mw}$ (Wang & Wu, 2004), that is, well beyond the Rankine vortex boundary at $r = R_{mw}$. The OR extends beyond $2R_{mw}$. Figure 2

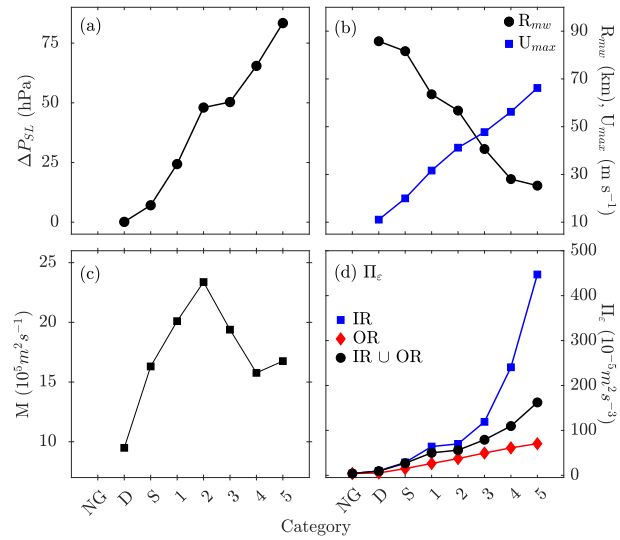

Figure 1. Storm parameters estimated from radial leg data versus storm intensity. The parameters are the mean values for each category. (a) ΔP_{SL}—the 0–500 km sea level pressure difference; (b) U_{max}—the maximum wind speed and R_{mw}—the radius of maximum wind; (c) $M = R_{mw}U_{max}$—the tropospheric level angular momentum; and (d) Π_ε—the magnitude of the horizontal energy flux estimated from the longitudinal spectra.

illustrates this subdivision and shows further subdivision of the IR into eyewall (light green, $r \le R_{mw}$) and near-core (pink, $R_{mw} < r \le 2\ R_{mw}$) regions. The bands over which the Kolmogorov slope was observed with satisfactory accuracy were in the range of 3–5 km for the full and Inner Regions and 3–20 km for the OR. Figure 1d shows the magnitudes of Π_ε estimated from longitudinal spectra over wavenumber bands from these ranges. In addition, the figure shows a superposition of all category 5 tangential wind profiles found in our data set with each profile normalized by its specific value of R_{mw}.

First of all, note that M and Π_ε exhibit different dependencies on storm intensity as shown in Figures 1c and 1d. As TCs nearly conserve their absolute angular momentum but do not conserve their KE, M and Π_ε are mutually independent. As a consequence, one has to distinguish between TC intensification in terms of Π_ε and in terms of U_{max}. The relationship between them is likely not very strong and nonuniversal.

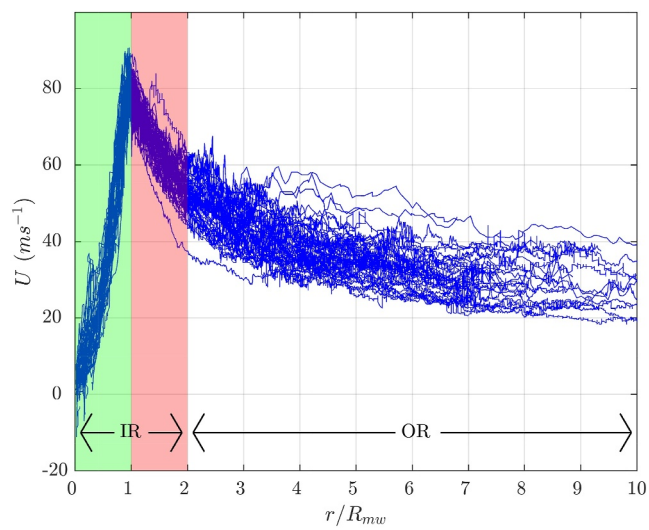

Figure 2. The tangential wind for all Cat 5 flight legs as a function of distance scaled by R_{mw}. The figure shows the division of the flow field into an inner region, comprised of the eyewall (light green), the near-core (pink), and the outer region.

21698996, 2025, 14, Downloaded from https://agupubs.onlinelibrary.wiley.com/doi/10.1029/2024JD042733, Wiley Online Library on [24/08/2025]. See the Terms and Conditions (https://onlinelibrary.wiley.com/terms-and-conditions) on Wiley Online Library for rules of use; OA articles are governed by the applicable Creative Commons License

21698996, 2025, 14, Downloaded from https://agupubs.onlinelibrary.wiley.com/doi/10.1029/2024JD042733, Wiley Online Library on [24/08/2025]. See the Terms and Conditions (https://onlinelibrary.wiley.com/terms-and-conditions) on Wiley Online Library for rules of use; OA articles are governed by the applicable Creative Commons License

Table 2
Parameter Values Estimated From the IR and Inner Region ∪ Outer Region Sample Sets

Category	Inner region						IR ∪ OR
	$\Pi_\varepsilon \times 10^5$ m^{2}s^{-3}	L_Ω (km)	L_β (km)	C_{fL}	C_{fT}	C_Z	$\Pi_\varepsilon \times 10^5$ (m^{2}s^{-3})
TD	9.8	1.48	18.98	0.040	0.030	0.00	9.4
TS	28.7	1.07	15.39	0.036	0.026	2.00	26.9
1	64.1	0.58	10.13	0.032	0.025	3.50	50.1
2	70.0	0.38	7.83	0.028	0.020	3.50	56.0
3	119.1	0.24	5.29	0.010	0.014	3.60	79.1
4	240.5	0.16	3.59	0.008	0.012	3.60	109.7
5	447.1	0.16	3.34	0.007	0.011	4.50	162.3

Note. These are used in Equations 10 and 11. Here, Π_ε is the horizontal energy flux; L_Ω is the Woods scale, and L_β is the transitional scale between the Kolmogorov and zonostrophic subranges in a 2D case when the peristrophic subrange is suppressed (Galperin et al., 2019).

Both Figures 1d and Table 2 indicate that the energy flux increases with storm intensity and reflects turbulence intensification due to such factors as increasing winds and turbulent air-sea enthalpy fluxes (Emanuel et al., 2023; Zhang et al., 2008). The values of Π_ε are approximately equal in the IR and OR for weak storms and exponentially increase with storm intensity, particularly in the IR, where they greatly exceed the values in the OR. When evaluated for IR ∪ OR, Π_ε acquires intermediate values between those in IR and OR. If Π_ε is chosen as a measure of a TC's destructive power, then the destruction potential reaches maximum inside the IR where Π_ε sharply increases after attaining the strength of Category 3.

Table 2 provides further insight into the behavior of Π_ε. In the Kolmogorov subrange, as expected, the values of Π_ε for tropical depressions and storms converge to those typical of tropospheric NG85 spectra $\sim 4 \times 10^{-5}$ m^{2}s^{-3}. They increase exponentially for storms of stronger intensity. Within the IR, Π_ε gradually rises by a factor of about 40 for storms ranging from tropical depression to Category 5. This information, and its quantitative aspect in particular, is important for hurricane wind risk assessment purposes, for example, Kantha (2008), and can be used in addition to other metrics such as maximum wind speed and storm size (Zhai & Jiang, 2014), a surge scale (Irish & Resio, 2010), and a quantile regression approach (Murnane & Elsner, 2012).

The values of Π_ε in Table 2 were obtained around flight altitudes, but most damage to buildings and properties is confined to the lower part of the boundary layer. Although more research is needed to relate the values of Π_ε at different altitudes, it is instructive to compare our values of Π_ε with those estimated by Byrne and Zhang (2013) in the boundary layers of Hurricanes Fabian (Category 4) and Isabel (Category 5) in September 2003 using third-order structure functions. For both hurricanes, the direction of energy transfer was found to change from direct to inverse at altitudes greater than about 100 m. For Isabel, the values of Π_ε were approximately 9×10^{-3} m^2 s^{-3} for altitudes below 100 m and approximately -2.5×10^{-3} m^2 s^{-3} for altitudes around 300 m. Of importance, these values have the same order of magnitude and their moduli differ by only an $O(1)$ factor. They compare favorably with our analysis that yields $\Pi_\varepsilon \sim 4.5 \times 10^{-3}$ m^2 s^{-3} as shown in Table 2 for Category 5 storms. A comparison with the data for Hurricane Fabian yielded similar results.

Table 2 provides estimates of the Woods scale. They are shorter than the mentioned earlier flight legs over which the values of Π_ε were evaluated, and so it is likely that Π_ε is mostly negative. Recall, however, that the spectra do not allow for the determination of the sign of Π_ε. Two additional pieces of information could be mentioned in this respect. First, studies by Tang et al. (2015) showed that Π_ε is mostly negative for $r < 1.5R_{mw}$ and positive for $r > 1.5R_{mw}$. The values of Π_ε in that study were, again, consistent with the present estimates by the order of magnitude. Second, in simulations of TCs by Oguejiofor et al. (2024), the *effective* horizontal eddy viscosity, whose sign can also be related to the direction of the energy transfer, was computed from numerical data. It was shown to change sign with both the horizontal distance from the TC center and the altitude with the inverse transfer prevailing on smaller scales.

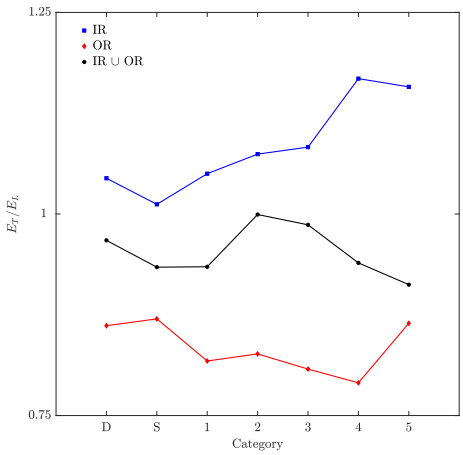

Figure 3. The ratio of the transverse and longitudinal spectra, E_T/E_L, estimated over wavenumber bands corresponding to the scale range 3–5 km as a function of storm intensity.

Finally, the state of TC turbulence on relatively small scales can be diagnosed in terms of the ratio, E_T/E_L. This ratio is shown on Figure 3 as a function of storm intensity category. It is greater than 1 (between 1 and 1.25) in the IR, less than 1 (between 0.75 and 1) in the OR, and slightly below 1 for the TC as a whole. Akin to the present OR values, aircraft-based observations in the atmospheric boundary layer yield $0.72 \lesssim E_T/E_L \lesssim 0.94$ (Nowak et al., 2025). On the other hand, one notes that on large scales outside the Kolmogorov subrange, $E_T/E_L > 1$ for all intensities, the property that points to the solenoidal nature of the flow field (Monin & Yaglom, 1975).

3.3. Spectra

Our calculations indicated that spectral amplitudes are sensitive to the scale intervals over which they are evaluated. To better understand this sensitivity, we computed the spectra in the IR and OR separately. Respective sample sets were created by subdividing flight legs at $r = 2R_{mw}$ and the ensuing spectra are elucidated in Section 3.4. To provide a better general overview of the spectra, they were evaluated over the entire range of flight legs denoted by IR ∪ OR, and they are shown here first. Section A3 details the procedure by which the spectra were calculated and shows three examples of computing the spectra for individual storms.

Figure 4 reveals a wealth of new information on the dynamics of hurricanes by considering their longitudinal and transverse spectra in the range IR ∪ OR. The figure compares observational spectra (solid lines) with Equations 10 and 11 (dashed lines). The analytical formulae for turbulence in hurricane winds have been hitherto unknown, and so the comparison appears here for the first time. Two main features are immediately obvious: the TC and tropospheric NG85 spectra are geometrically congruent and the amplitudes of the TC spectra monotonically increase with storm intensity. These two traits settle the previously identified similarity and dissimilarity in the behavior of TC and tropospheric spectra.

The contrast between the longitudinal and transverse spectra in Figure 4 is startling. In conformity to Equations 10 and 11, E_L is consistent with the peristrophic regime whereas E_T acquires the steep zonostrophic slope. At first sight, the spectra appear to pertain to different flows, yet they merely reflect the fusion of the peristrophic and zonostrophic regimes of rotating turbulence embedded in the above two equations. The large dots on both spectra

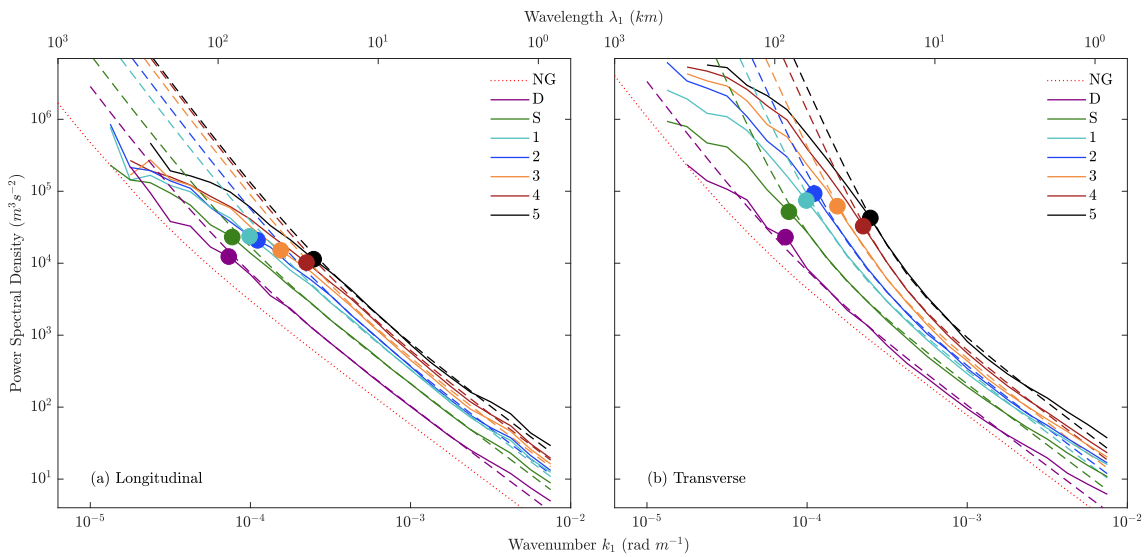

Figure 4. Longitudinal (a) and transverse (b) wavenumber spectra computed over the union of inner and outer regions. The dashed lines represent the composite spectra, Equations 10 and 11. The red dotted lines are QNSE-predicted NG85 spectra, Equations 4 and 5, for $\phi = 25°$N and $\Pi_\varepsilon = 4 \times 10^{-5} m^2 s^{-3}$, see Galperin and Sukoriansky (2020). The large dots on the spectra mark the length scale R_{mw}.

21698996, 2025, 14, Downloaded from https://agupubs.onlinelibrary.wiley.com/doi/10.1029/2024JD042733, Wiley Online Library on [24/08/2025]. See the Terms and Conditions (https://onlinelibrary.wiley.com/terms-and-conditions) on Wiley Online Library for rules of use; OA articles are governed by the applicable Creative Commons License

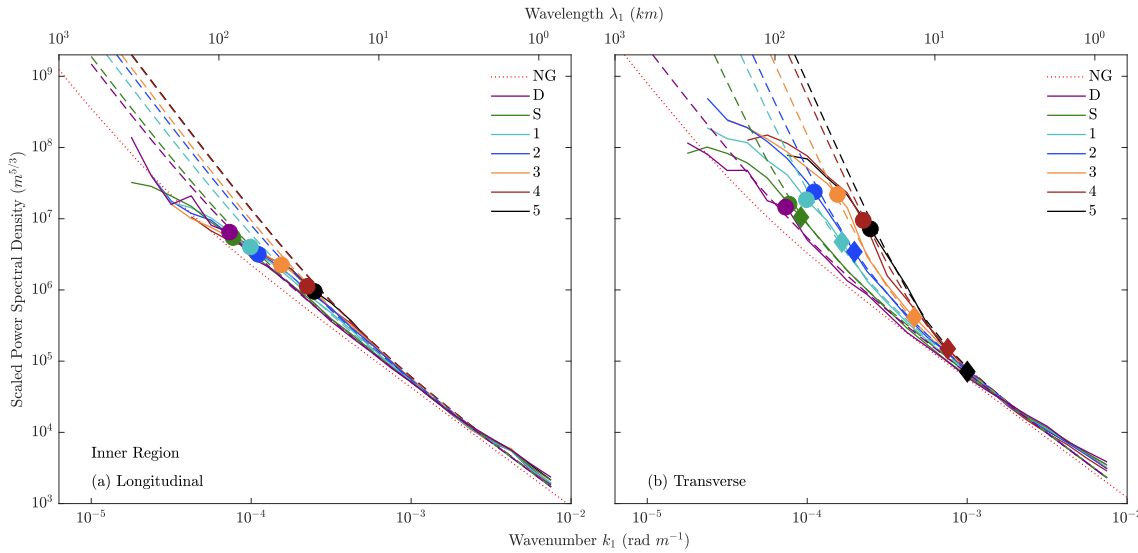

Figure 5. Longitudinal (a) and transverse (b) wavenumber spectra for the inner region samples. The dashed lines represent composite spectra given by Equations 10 and 11. The red dotted lines are the quasi-normal scale elimination predicted NG85 spectra (Equations 4 and 5) for $\phi = 25°$N and $\Pi_\varepsilon = 4 \times 10^{-5}$ m^2 s^{-3} (Galperin & Sukoriansky, 2020). The large dots indicate spectral amplitudes at $\lambda_1 = R_{mw}$ whereas the large diamonds on (b) correspond to the wavelength L_{PZ} given by Equation 16 and marking the boundary between the peristrophic and zonostrophic subranges. Each spectrum has been normalized with the respective value of $\Pi_\varepsilon^{2/3}$.

mark the values of R_{mw} as given in Table 1. Consistently with Figure 1b, they reflect the decrease of R_{mw} with increasing storm intensity.

Apparently, R_{mw} coincides with the terminus of the zonostrophic regime for all storm categories. This important result underscores the significance of R_{mw} beyond being the radius of maximum wind. On scales larger than R_{mw}, $\hat{f}$ and $\hat{\beta}$ decrease and the growth of the spectral amplitudes slows down. Eventually, both E_L and E_T merge with their respective NG85 counterparts at the TC vortex periphery.

One could think that the merging scales of TC and NG85 spectra could be utilized as an alternative definition of the external scale of a TC vortex, compare e,g. with Chavas et al. (2016). Such definition is problematic, however, because the longitudinal and transverse spectra would yield different values for such a scale.

The values of the coefficients in Equations 10 and 11 as estimated from the spectra are collected in Table 2. Evidently, C_{fL} and C_{fT} decrease with increasing $\hat{f}$ whereas $C_Z \simeq 2$ remains practically invariant in a broad range of variation of $\hat{f}$ and $\hat{\beta}$. This is an important result because for the zonostrophic regime on Jupiter, Cassini observations yielded $C_Z \simeq 2$ (Galperin et al., 2014). The peristrophic regime, on the other hand, serves as a glue ensuring a smooth transition between the zonostrophic and Kolmogorov subranges. The details of the interaction between these three regimes are not clear and require further investigation. Among the issues that need clarification is the decrease of C_{fL} along with C_{fT} with increasing $\hat{f}$ even though the zonostrophic term is explicitly present only in the transverse spectra.

Figure 4 makes it clear that the understanding and prediction of the behavior of TCs requires consideration of both longitudinal and transverse spectra in tandem. A horizontally integrated 2D spectrum, such as that used by Green and Zhang (2015), is insufficient to account for spectral anisotropy. Regarding the spectral steepness, it plays a major role in issues related to predictability of atmospheric phenomena (Lorenz, 1963, 1969) and, in particular, predictability of TCs (Kieu & Rotunno, 2022). The papers by Lorenz (1963, 1969) dealt with isotropic 2D turbulence. In the light of our new results, the applicability of the preceding studies to strongly anisotropic atmospheric and planetary flows requires reassessment.

The difference between the longitudinal and transverse spectra is further accentuated in Figure 5 where the individual spectra computed over the inner region are normalized with their respective values of $\Pi_\varepsilon^{2/3}$. This normalization collapses all lines in the Kolmogorov subrange into a single curve that illuminates the existence and the extent of that subrange. The subrange shrinks with increasing storm intensity despite the boost of Π_ε.

21698996, 2025, 14, Downloaded from https://agupubs.onlinelibrary.wiley.com/doi/10.1029/2024JD042733, Wiley Online Library on [24/08/2025]. See the Terms and Conditions (https://onlinelibrary.wiley.com/terms-and-conditions) on Wiley Online Library for rules of use; OA articles are governed by the applicable Creative Commons License

21698996, 2025, 14, Downloaded from https://agupubs.onlinelibrary.wiley.com/doi/10.1029/2024JD042733, Wiley Online Library on [24/08/2025]. See the Terms and Conditions (https://onlinelibrary.wiley.com/terms-and-conditions) on Wiley Online Library for rules of use; OA articles are governed by the applicable Creative Commons License

Subrange diminution is stipulated by the decrease of R_{mw} and expansion of the zonostrophic subrange as elaborated in the next subsection. Storm compaction along with the spectral steepening are behind the observed by Vonich and Hakim (2018) shifting of the transition zone between the steep and mild spectral slopes downscale with increasing TC category.

3.4. The Rhines Scale

Upon having established the presence of the zonostrophic regime in TC vortices, recall that an important characteristic of this regime is the Rhines scale that provides a measure of the width of zonal jets,

$$L_{Rh} = \left(\frac{2U}{\beta}\right)^{1/2}, \tag{14}$$

where U is the rms velocity, and β is the planetary β. A detailed study of the Rhines scale in the planetary context can be found in the book by Galperin and Read (2019).

In a series of numerical experiments, Lu and Chavas (2022) found that a TC vortex size is limited by the Rhines scale based upon the planetary β. Here, in Section 2, it was established that for the IR of a TC vortex, cyclostrophic, and planetary β-effects are basically decoupled, and so one can introduce a vortex Rhines scale based upon $\hat{\beta}$,

$$L_{Rh} = \left(\frac{2U_{max}}{\hat{\beta}}\right)^{1/2} = R_{mw}. \tag{15}$$

This equation could also be derived following Sukoriansky et al. (2007) by integrating the zonostrophic spectrum to the maximum scale in the zonostrophic subrange. It establishes an inherent similarity between the regimes of vortex zonostrophic turbulence developing in the IR of a TC and zonostrophic turbulence in global Jovian circulations. In both cases, the regime manifests in formation and maintenance of zonal jets. What is the physical underpinning of this similarity and what is the TC equivalent of a zonal jet?

The azimuthal velocity profile in a TC shown in Figure 2 resembles an eastward zonal jet on Jupiter or Saturn. In a TC vortex, changes in $\hat{f}$ give rise to the differential rotation that drives the cyclostrophic β-effect. Either cyclostrophic or planetary β-effect acts to establish the regime of zonostrophic turbulence with its characteristic steep anisotropic spectrum and zonal jets whose width scales with L_{Rh}. This conclusion is explored in the next Subsection.

3.5. The Eyewall as an Equivalent Zonal Jet

To investigate the nature of turbulence in different regions of a TC vortex, we computed transverse spectra over three types of flight legs that belong in the following ranges: (a) $(0, R_{mw})$, (b) $(0, 1.5R_{mw})$, and (c) $(0, 2R_{mw})$. All spectra are shown on Figure 6. Surprisingly, even though, according to Figure 4, the zonostrophic regime extends up to a scale R_{mw}, the spectra in the range (a) do not rise to the zonostrophic slope. Consideration of the ranges (b) and (c) resolves this inconsistency as they clarify that the zonostrophic subrange occupies the domain between $\sim 0.5R_{mw}$ and $\sim 1.5R_{mw}$. As the turbulence in this domain is in the zonostrophic regime and the domain's width is approximately equal to R_{mw} or, by Equation 15, to L_{Rh}, we conclude that the jet-like TC flow between $\sim 0.5R_{mw}$ and $\sim 1.5R_{mw}$, shown on Figure 2, is isomorphic to a Jovian zonal jet. As this vortex domain is a residence of the eyewall, we conclude that a TC eyewall is a virtual equivalent of the Jovian zonal jet.

Visual comparison of the observational spectra with the reference slopes in Figure 6 shows that neither of the spectra attains a hypothesized slope exactly. As mentioned earlier, the superposition of the three possible spectral slopes in Equation 11, that is, $-5/3$, -3 and -5, can accommodate nearly any slope in between dependent on the positions of the concatenation points. The onus in these comparisons was put on the agreement for the amplitudes rather than the slopes. With this in mind, fitting the composite and observed spectral profiles allowed us to estimate the empirical constants as explained in the Subsection 3.3. It needs to be emphasized that a good agreement between the observational and composite spectra given by Equations 10 and 11 could only be achieved with all terms in these equations being engaged.

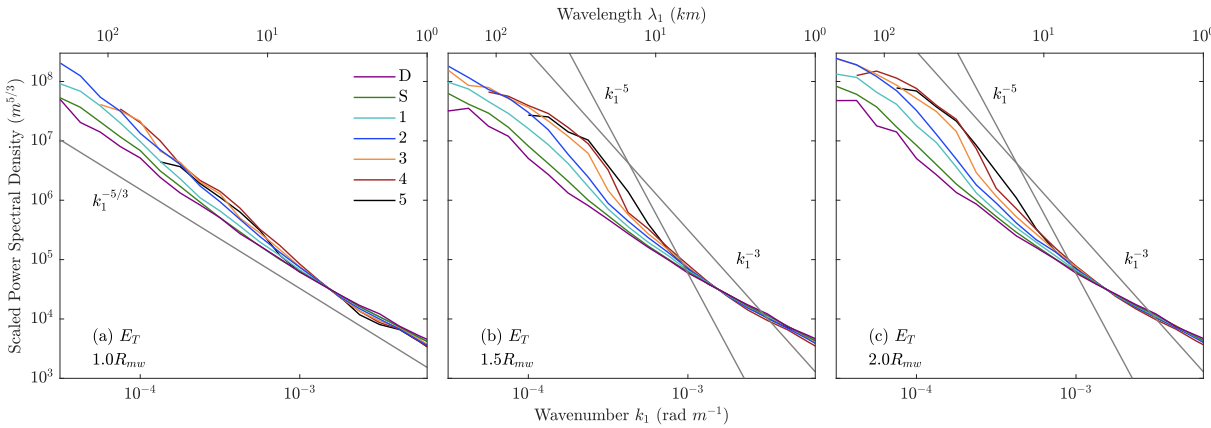

Figure 6. Transverse spectra computed over different radial segments: (a) $(0, R_{mw})$, (b) $(0, 1.5R_{mw})$, and (c) $(0, 2R_{mw})$. The spectra have been scaled with their respective estimates of $\Pi_\varepsilon^{2/3}$. Every panel shows relevant reference slopes.

3.6. The Vortical Hot Towers

A TC eyewall contains a sequence of tall thunderstorms that produce heavy rains and the strongest winds. It may contain large hot vortices known as Vortical Hot Towers or VHT. They may participate in the cyclogenesis or be produced by a developing storm, for example, Montgomery et al. (2006), Montgomery and Smith (2017). A comprehensive analysis of the dynamics and thermodynamics of VHTs would exceed the barotropic framework employed in this study. However, turbulent processes in this system have not received sufficient attention so far despite their importance, and so this Subsection will highlight some of them.

From the viewpoint of turbulence, a system comprised of an eyewall, or, as elaborated in the preceding Subsection, an equivalent zonal jet, and a sequence of large embedded vortices has been studied in laboratory experiments and in its manifestations in the atmospheres of the giant planets. Many examples of such a system were considered in Part III of the book by Galperin and Read (2019). Additional experimental studies were conducted more recently by Lemasquerier et al. (2023). Most of the experiments employed a topographic β-effect, and the resulting flows approached the zonostrophic regime. To the best knowledge of the authors, vortex Rossby waves have not been studied in a laboratory. In some of the experiments, turbulence was excited and maintained by small-scale jets injected at the bottom of a device. Other experiments employed convective forcing (Chapter 7 in Galperin and Read (2019)). Such a forcing can be viewed as an analog of mesovortices or tornadoes energizing hurricane cores or flows in the eyewalls (Montgomery et al., 2006; Wurman & Kosiba, 2018). Some of these experiments can be used to study the interaction of vortex systems with zonostrophic turbulence. Experiments by Montgomery et al. (2002) were specifically designed to emulate VHTs mechanically, but they excluded the effect of the vortex Rossby waves.

Among other experiments, we recall those utilizing magnetohydrodynamic forcing with an electric current running through a salt solution and small circular magnets placed under the bottom surface, as described in Chapter 9 by Galperin and Read (2019). The resulting electromagnetic force generated small-scale vortices. The magnets were placed either in a grid, to produce a space-distributed forcing, or in an arc, to generate a zonal jet directly. Most of the experiments with a topographic β-effect produced the regime of zonostrophic turbulence in a cylindrical coordinate system. The main principal difference between these experiments and flows in TCs was that in the former, a β-effect was produced by external factors and so β remained constant while in the latter, β is produced by the cyclostrophic rotation and depends on the flow. These and other experiments underscored the important role of the anisotropic inverse energy transfer into the zonal mode that governs the regime of zonostrophic turbulence.

Two examples of the interaction between zonal jets and vortex systems in the zonostrophic regime are also relevant in the present context. Sánchez-Lavega et al. (2008) observed a single planetary-scale disturbance giving rise to a deep zonal jet on Jupiter. Although this phenomenon is likely analogous to a β-plume, see for example, Chapter 17 by Galperin and Read (2019), parallels can be drawn to the dynamics of VHTs. Another example is a single cyclone on Saturn observed by Gunnarson et al. (2023). Multiple convective storms were detected within

21698996, 2025, 14, Downloaded from https://agupubs.onlinelibrary.wiley.com/doi/10.1029/2024JD042733, Wiley Online Library on [24/08/2025]. See the Terms and Conditions (https://onlinelibrary.wiley.com/terms-and-conditions) on Wiley Online Library for rules of use; OA articles are governed by the applicable Creative Commons License

the cyclone. Note that the circulation on Saturn also spotlights a zonostrophic regime. Clearly, VHTs and mesovortices are driven by complicated thermodynamics and moisture transformation processes whose effects go beyond purely mechanical forcing. However, the anisotropic inverse energy transfer and energy accumulation in the zonal mode are processes of paramount importance that have been underappreciated in studies of the dynamics of TCs. A more detailed picture of the interaction between VHTs and TC vortices could emerge from computing the energy spectra of TCs and estimating the energy fluxes associated with the forcing by VHTs.

3.7. The Boundary Between the Peristrophic and Zonostrophic Ranges

The characteristic timescales of the peristrophic $\left(\tau_p = \hat{f}^{-1}\right)$ and zonostrophic $\left(\tau_z = \hat{\beta}^{-1}k_1\right)$ regimes delineate the domains of their predominance. Using Equation 11, one can find a scale, L_{PZ}, marking the boundary between the respective ranges as a function of R_{mw} related to a storm category via Table 2,

$$L_{PZ} = \left(\frac{C_{fT}}{C_Z}\right)^{1/2} R_{mw}. \tag{16}$$

The values of C_{fT} and C_Z are tabulated in Table 2. The zonostrophic regime prevails for $k_1 < 2\pi/L_{PZ}$ whereas the peristrophic regime is dominant for $k_1 > 2\pi/L_{PZ}$. The boundary (Equation 16) is marked by large diamonds on Figure 5. Evidently, L_{PZ} decreases with increasing intensity, and for categories 4 and 5, it is pushed almost into the Kolmogorov subrange. Such interaction of the subranges is stipulated by the behavior of the coefficients C_{fT} and C_Z—although the former decreases, the latter remains nearly invariant for all categories. In summary, as R_{mw} shrinks and the transverse spectra steepen with escalating category, the swelling zonostrophic subrange vanquishes its peristrophic neighbor by pushing it deeper and deeper into the Kolmogorov subrange. In the context of Earth's tropical storms, Figure 5b traces a transition from purely peristrophic flow regimes with the NG85—MOZAIC spectra to mixed peristrophic—zonostrophic ones and to the penultimate reign of vortex zonostrophic turbulence.

As a consequence of the disappearance of the peristrophic subrange, a flow acquires features of 2D turbulence with a β-effect. This explains the success of early studies of zonostrophic turbulence using 2D models, see for example, Chapter 13 of Galperin and Read (2019). From these studies, a criterion of the threshold of the zonostrophic regime was derived in terms of the *zonostrophy index* R_β,

$$R_\beta \simeq 0.5\,\frac{L_{Rh}}{L_\beta}. \tag{17}$$

For storms of Categories 4 and 5, the zonostrophy index is about 3.5 and 4. The threshold value is about 2.5, while for Jupiter and Saturn that boast strong zonal jets, $R_\beta \sim 5 - 6$. It is remarkable that the regime of zonostrophic turbulence develops in strong Earth's hurricanes.

3.8. The Kolmogorov Subrange

The sensitivity of the spectra to the position of the inner radius of the OR is investigated in Figure 7. The figure shows normalized spectra for an OR with its inner boundary placed at R_{mw}, $2R_{mw}$, and $3R_{mw}$. The purpose of this figure is to uncover turbulence modifications by cyclostrophic rotation with increasing distance away from the storm center. As the radius increases and the azimuthal velocity decreases, the angular velocity of the cyclostrophic rotation decreases as well, and its influence fades away. Evidently, all spectra feature the Kolmogorov regime with the exception of the transverse spectrum on Figure 7b that reveals a weak peristrophic regime.

One may wonder about the ubiquity of the Kolmogorov subrange in turbulence that is neither homogeneous nor isotropic. An insightful resolution of this conundrum was offered by Kolmogorov (1934) who attributed the spectrum with the $-5/3$ exponent to processes that can be classified as the random walk. Golitsyn (2018) expanded this analysis in an article with an ambitious title "Random Walk Laws by A.N. Kolmogorov as the Basics for Understanding Most Phenomena of the Nature."

21698996, 2025, 14, Downloaded from https://agupubs.onlinelibrary.wiley.com/doi/10.1029/2024JD042733, Wiley Online Library on [24/08/2025]. See the Terms and Conditions (https://onlinelibrary.wiley.com/terms-and-conditions) on Wiley Online Library for rules of use; OA articles are governed by the applicable Creative Commons License

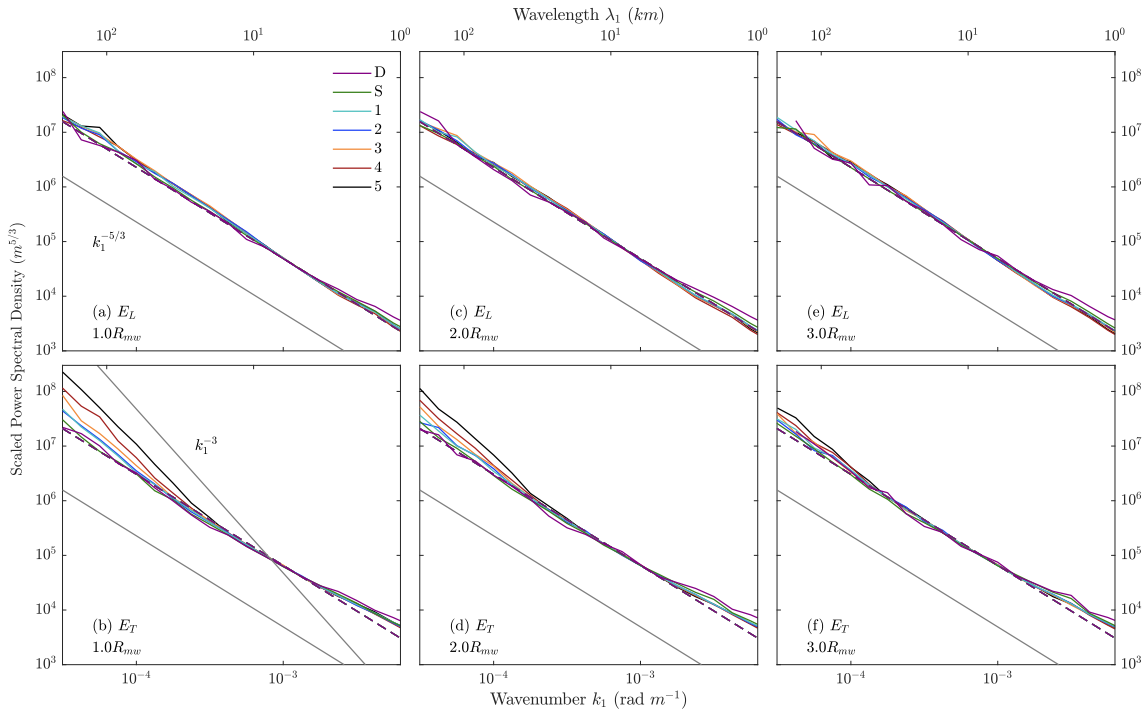

Figure 7. Longitudinal (a, c, e) and transverse (b, d, f) wavenumber spectra for different parts of the OR: (a) and (b) $r > R_{mw}$, (c) and (d) $r > 2R_{mw}$, and (e) and (f) $r > 3R_{mw}$. The dashed lines are composite spectra given by Equations 10 and 11. The spectra have been scaled with their respective estimates of Π_ε. A $k^{-5/3}$ reference slope is drawn in each panel (solid gray line).

4. Conclusions

This paper presents a comprehensive study of anisotropic TC turbulence in a barotropic framework. It utilizes a well-known concept of the Rankine vortex that extends to the radius of maximum wind beyond which the azimuthal velocity decreases with the distance away from the storm center. A linear deviation from the basic flow in the IR produces a cyclostrophic β-effect that supports vortex Rossby waves. These waves render turbulence anisotropic with vastly different KE spectra in the azimuthal and radial directions. Those are also the longitudinal and transverse spectra of the azimuthal velocity fluctuations.

The study makes it clear that in order to expose the intricacies of the anisotropic TC turbulence, its longitudinal and transverse spectra must be investigated in tandem. This proved to be a critical modus operandi because each one of these 1D spectra alone could point to a different flow regime. In addition, spectral amplitudes in our analysis were given at least as much attention as the slopes.

In summary, the main conclusions of this study are:

1. The cyclostrophic Coriolis parameter, $\hat{f}$, exceeds its planetary counterpart, f, by a factor of, approximately, from 5 for a tropical depression to 100 for category 5 hurricanes. In the same range of storms, the cyclostrophic β exceeds planetary β by a factor varying from 10^2 to 10^4. Thus, as far as storms are concerned, their large-scale cyclostrophic dynamics is decoupled from the planetary counterpart;
2. On relatively small scales, the spectra in all regions obey the Kolmogorov law, yet the direction of the energy transfer is unknown and may change with the altitude and the horizontal distance. Future research based upon the analysis of the third order structure functions will provide tools for determination of both the sign and the magnitude of Π_ε;
3. Most energy dissipation takes place inside the IR. Its rate, $\varepsilon \simeq \Pi_\varepsilon$, is one of the products of the current spectral analysis. An estimate cited by Kantha (2008) relates the wind damage sustained by a structure to the rate of work done by the wind destructive potential which can be related to ε. As evident from Figure 1d, the increase of Π_ε with the storm intensity and with U_{max} is exponential. Recall that Murnane and Elsner (2012) found that the relationship between hurricane losses and wind speed is also exponential. Thus, as suggested by

21698996, 2025, 14, Downloaded from https://agupubs.onlinelibrary.wiley.com/doi/10.1029/2024JD042733, Wiley Online Library on [24/08/2025]. See the Terms and Conditions (https://onlinelibrary.wiley.com/terms-and-conditions) on Wiley Online Library for rules of use; OA articles are governed by the applicable Creative Commons License

21698996, 2025, 14, Downloaded from https://agupubs.onlinelibrary.wiley.com/doi/10.1029/2024JD042733, Wiley Online Library on [24/08/2025]. See the Terms and Conditions (https://onlinelibrary.wiley.com/terms-and-conditions) on Wiley Online Library for rules of use; OA articles are governed by the applicable Creative Commons License

Kantha (2008), there should exist a simple relationship between hurricane losses and Π_ε. This relationship and its derivatives that will be established in future research may find a range of applications in hurricane wind damage assessment and its prediction;

4. We distilled a new regime developing in rotating flows with a constant angular velocity. This regime was termed *peristrophic*. Spectral amplitudes in this regime are proportional to $f^2k_1^{-3}$ rather than $\eta^2k_1^{-3}$, η being the rate of the enstrophy transfer as suggested in the theory of geostrophic turbulence by Charney (1971);
5. When a β-effect is also present, it evokes the zonostrophic regime. We demonstrated that the TC turbulence can be represented by superposition of these two regimes. Using TC data, we investigated their interaction in the range of two orders of magnitude of the Coriolis parameter. The interaction was analyzed in terms of the longitudinal and transverse spectra;
6. On small scales, both spectra are Kolmogorov-like. On larger scales, both spectra steepen to the peristrophic k_1^{-3} exponent. On even larger scales, the transverse spectra acquire the zonostrophic exponent, k_1^{-5}, whereas the longitudinal spectra preserve their peristrophic slope. The zonostrophic regime is produced by the anisotropic inverse energy transfer into a zonal or null-mode. This is a basic phenomenon germane to rotating flows with a β-effect produced by either curvilinear geometry or differential rotation. The spectral anisotropy was demonstrated and quantified in this study for the first time;
7. The generalization of the peristrophic regime to vortex flows by virtue of superposing the cyclostrophic and planetary Coriolis parameters explains the observed affinity of the TC and tropospheric NG85 spectra and recovers the monotonic rise of spectral amplitudes with the storm category;
8. As $\tilde{f} \to f$ on scales corresponding to the vortex edge, the TC and the NG85—MOZAIC spectra tend to merge. This asymptotic behavior is demonstrated here for the first time. This demonstration was enabled by the analytical expressions derived for the tropospheric spectra in the framework of the QNSE theory;
9. The near-conservation of the absolute angular momentum, M, facilitates compaction of IR and the eyewall region with increasing storm intensity. The zonostrophic range expands and impinges farther and farther into its peristrophic neighbor causing its contraction. Eventually, for very strong storms, the zonostrophic range may completely expunge the peristrophic one. The resulting IR may then encompass the zonostrophic and Kolmogorov ranges only and appear to feature 2D turbulence with a β-effect;
10. The width of the eyewall region forming a jet in the azimuthal velocity profile is scaled with the vortex Rhines scale. This scale is akin to the Rhines scale in planetary flows and underscores the similarity of zonostrophic regimes in vortex and planetary flows;
11. By virtue of scaling with the vortex Rhines scale and featuring the zonostrophic energy spectrum, the eyewall region of a TC can be identified as a virtual equivalent of a zonal jet;
12. A broad range of variation of $\hat{f}$ and $\hat{\beta}$ germane to the tropical storms sweeps through the entire range of regimes of cyclostrophic turbulence as they progress, with increasing storm intensity, from purely peristrophic to mixed peristrophic-zonostrophic to predominantly zonostrophic.

Appendix A: Data and Methods

A1. Reconnaissance and Best Track Data

The present analysis utilized data from about 3,000 hurricane reconnaissance missions into 320 tropical systems in the North Atlantic and eastern Pacific Oceans from 1977 to 2022. The flights were conducted by the National Oceanic and Atmospheric Hurricane Administration (NOAA) Hurricane Hunters and the U.S. Air Force (USAF) Reserve Command 53rd Weather Reconnaissance Squadron.

Instruments on the reconnaissance aircraft measured (at 1, 10, or 60 s intervals): wind speed (±4 kt; 1 kt = 0.51 ms^{-1}), wind direction (±10°), GPS position (±3 n.mi; 1 n.mi = 1.85 km), flight speed, altitude, sea level pressure, and other variables; for further details, see Vonich and Hakim (2018). Quality control was applied to remove flight data duplication, data contaminated by GPS failure, and failures of the wind measuring instrument.

NOAA Best Track was used to obtain a history of storm position, storm intensity (maximum estimated 60 s sustained wind speed), and central pressure. More precise storm tracks, at approximately 2 min time steps, were created by HRD of the Atlantic Oceanographic and Meteorological Laboratory by combining the NBT, the reconnaissance data (including radar), satellite, and other data. In cases where it was determined that the storm was tilted, different track files were created. The HRD track was used for the storm position and the NBT for the

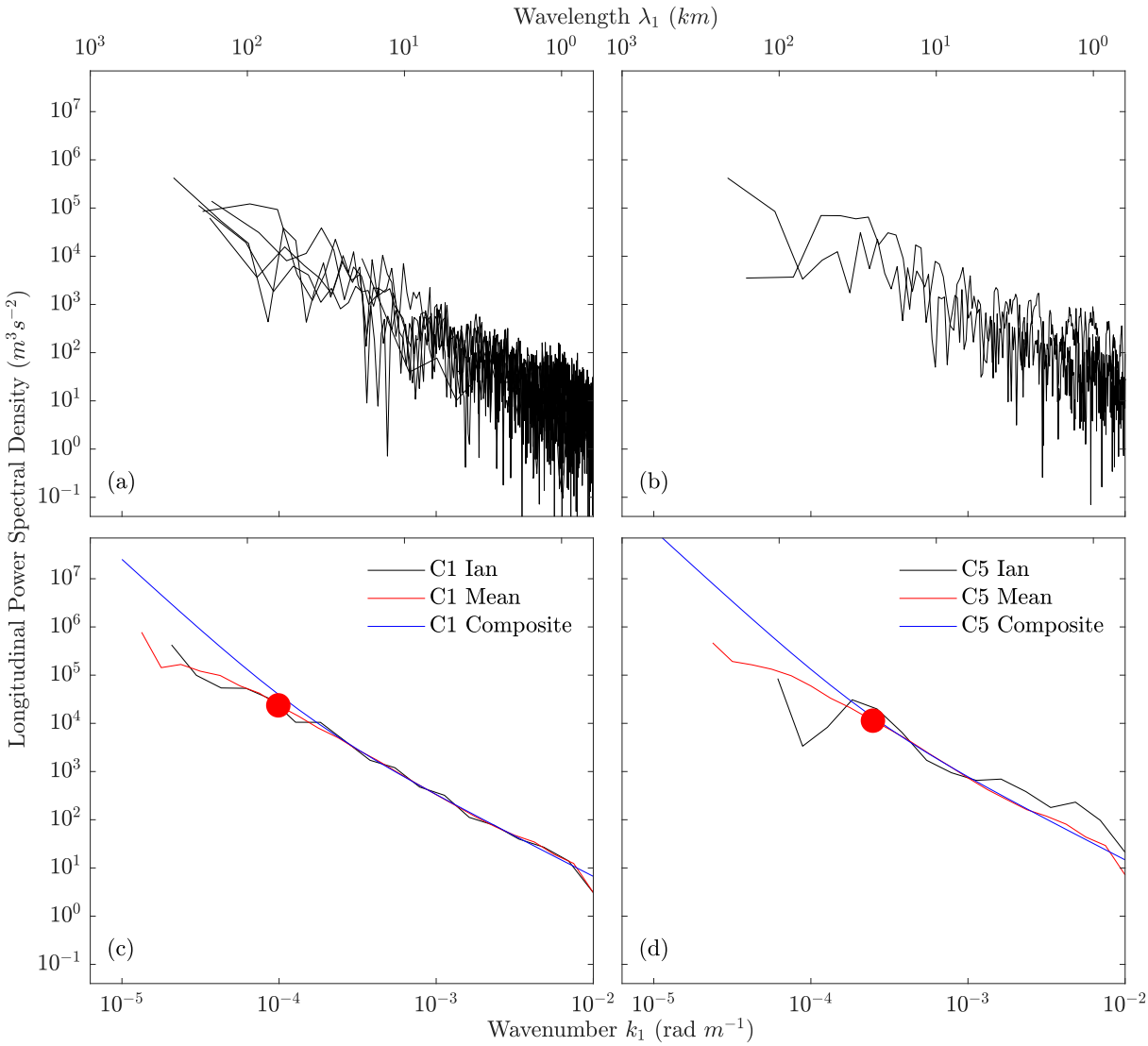

Figure A1. Longitudinal spectra for the union of the inner and outer regions from reconnaissance flights in Hurricane Ian (2022). (a) Individual flight leg spectra from flight 20220926H1, when Ian was a Category 1 storm. (b) Individual flight leg spectra from flight 20220928H1, when Ian was a Category 5 storm. (c) Binned and averaged spectra from flight 20220926H1 (black), binned and averaged spectra from all Category 1 flight legs in the data set (red), and predicted composite spectrum, Equation 10 (blue). (d) Same as in (c) but for Category 5. The large dot represents the radius of maximum wind, R_{mw}.

other variables. The combined track was interpolated to 1s using a cubic function for storm position and a linear interpolant for the wind and central pressure. This combined product will be referred to as the interpolated best track (IBT).

A2. Mission and Flight Leg Storm Parameters

Missions were classified based on the Saffir-Simpson scale using the IBT maximum interpolated wind. This was done for simplicity, knowing that intensity change is a nonlinear process, for example, Judt et al. (2023).

Mission data were processed to obtain estimates of key parameters, which were then averaged per category to obtain the mean 60-s sustained maximum tangential wind speed (U_{max}), the radius of maximum wind (R_{mw}), the storm center latitude (ϕ) and longitude, and the sea level pressure difference between 500 km and the storm center (ΔP_{SL}).

21698996, 2025, 14, Downloaded from https://agupubs.onlinelibrary.wiley.com/doi/10.1029/2024JD042733, Wiley Online Library on [24/08/2025]. See the Terms and Conditions (https://onlinelibrary.wiley.com/terms-and-conditions) on Wiley Online Library for rules of use; OA articles are governed by the applicable Creative Commons License

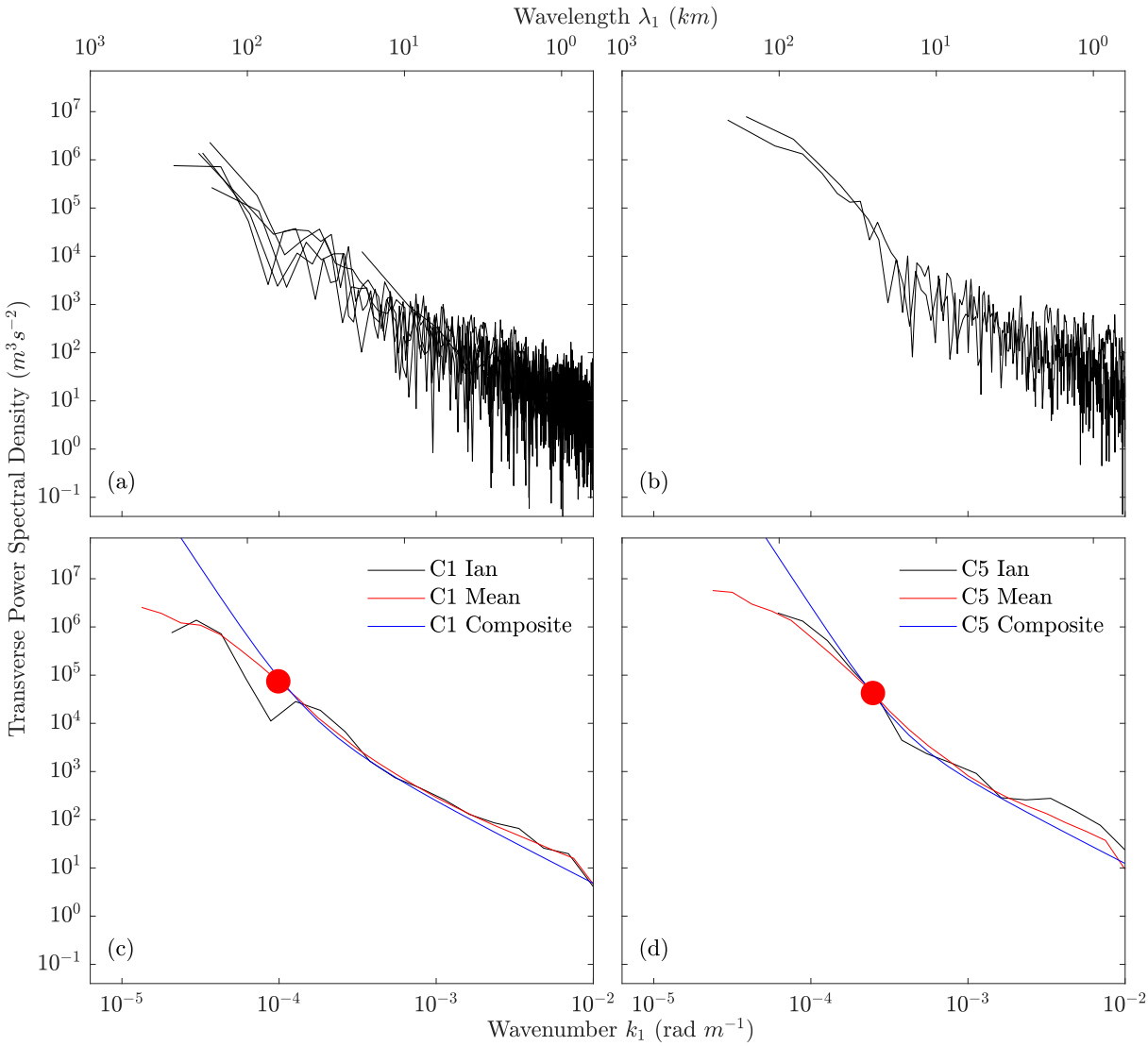

Figure A2. Same as in Figure A1 but for transverse spectra and predicted composite spectrum, Equation 11.

Flight patterns from each mission were parsed and trimmed to obtain *radial legs* (flight legs along radial lines). Only those legs with lengths greater than 10 km and passed within 25 km of the storm center were used.

A3. Calculating Spectra

Wind speed and wind direction were transformed to radial and azimuthal velocities in a storm-centered coordinate system. Spectra were calculated from flight leg samples based on the periodogram. The amplitudes were normalized by $\Delta r(2\pi N_s)^{-1}$ where N_s is the number of points in the sample and Δr is the grid spacing. The grid spacing for a flight leg is defined as the plane's average airspeed times the sampling interval. Since each flight leg has a unique average speed, Δr varied from sample to sample. In addition, flight legs were of varying length and hence N_s varied as well.

Samples were detrended by subtracting the line that connects the first and last points of the sample. This method of detrending eliminates the need for a window function to reduce spectral leakage. On the other hand, it does reduce spectral amplitudes at the largest scales (Errico, 1985; Vogelzang et al., 2011).

21698996, 2025, 14, Downloaded from https://agupubs.onlinelibrary.wiley.com/doi/10.1029/2024JD042733, Wiley Online Library on [24/08/2025]. See the Terms and Conditions (https://onlinelibrary.wiley.com/terms-and-conditions) on Wiley Online Library for rules of use; OA articles are governed by the applicable Creative Commons License

21698996, 2025, 14, Downloaded from https://agupubs.onlinelibrary.wiley.com/doi/10.1029/2024JD042733, Wiley Online Library on [24/08/2025]. See the Terms and Conditions (https://onlinelibrary.wiley.com/terms-and-conditions) on Wiley Online Library for rules of use; OA articles are governed by the applicable Creative Commons License

Spectra were combined by binning them into 20 logarithmically spaced bins between 10^{-5} and 10^{-2} rad m^{-1}. The binned spectra were grouped by storm intensity category and averaged. Examples of spectra before and after binning are shown in Figures A1 and A2 and compared to the average spectra for the storm category and the composite spectra. The constants in the equations are the same as those shown in Table 2.

Data Availability Statement

All data used in this study are available from the NOAA Atlantic Oceanographic and Meteorological Laboratory HRD website: https://www.aoml.noaa.gov/data-products/.

Acknowledgments

The authors would like to thank Trent Vonich for his assistance in acquiring the data and establishing the methods used in this study. Thanks also go to Dennis Mayer for his assistance in generating the spectra and Ralph Foster and Georgi Sutyrin for useful discussions. Support to Alexander K. Nickerson was provided by the NOAA ECOHAB program (award NA19NOS4780183), NOAA/IOOS through the Southeast Coastal Ocean Observing Regional Association (SECOORA, award NA21NOS0120097), NOAA Office of Coast Survey through the Center for Ocean Mapping and Innovative Technologies (COMIT, award NA20NOS4000227), and the State of Florida through FWC/FWRI (agreement # 20035). He also benefited from the Sanibel-Captiva Shell Club/Mary and Al Bridell Memorial Fellowship. Partial funding was provided by the NASA/NOAA Ocean Surface Topography Science Team and the National Science Foundation under Grant NSF PHY-1748958. Jun A. Zhang acknowledges support from NOAA Grant NA22OAR4050669D, National Science Foundation (NSF) Awards 2228299 and 2211308, and ONR MURI Grant N00014-24-1-2554. We also thank the organizers of the workshop "Rotating Turbulence: Interplay and Separability of Bulk and Boundary Dynamics" and its leader, Jonathan Aurnou that took place at UCLA in January 2025 where our results were presented, discussed, expanded, and enriched via communication with the Workshop participants. We also would like to thank the anonymous reviewers for their helpful comments that improved this manuscript.

References

Acheson, D. J. (1990). *Elementary fluid dynamics*. Oxford University Press.

Adem, J., & Lezama, P. (1960). On the motion of a cyclone embedded in a uniform flow. *Tellus*, *12*(3), 255–258. https://doi.org/10.3402/tellusa.v12i3.9405

Anthes, R. A., & Hoke, J. E. (1975). The effect of horizontal divergence and the latitudinal variation of the Coriolis parameter on the drift of a model hurricane. *Monthly Weather Review*, *103*(9), 757–763. https://doi.org/10.1175/1520-0493(1975)103<0757:teohda>2.0.co;2

Battalio, J. M., & Lora, J. M. (2021). Annular modes of variability in the atmospheres of Mars and Titan. *Nature Astronomy*, *5*(11), 1139–1147. https://doi.org/10.1038/s41550-021-01447-4

Bierdel, L., Snyder, C., Park, S.-H., & Skamarock, W. (2016). Accuracy of rotational and divergent kinetic energy spectra diagnosed from flight-track winds. *Journal of the Atmospheric Sciences*, *73*(8), 3273–3286. https://doi.org/10.1175/jas-d-16-0040.1

Biri, S., Serra, N., Scharffenberg, M. G., & Stammer, D. (2016). Atlantic sea surface height and velocity spectra inferred from satellite altimetry and a hierarchy of numerical simulations. *Journal of Geophysical Research: Oceans*, *121*(6), 4157–4177. https://doi.org/10.1002/2015JC011503

Boffetta, G. (2023). Dimensional transitions in turbulence: The effects of rotation and stratification. *MDPI Atmosphere*, *14*(11), 1688. https://doi.org/10.3390/atmos14111688

Boffetta, G., Celani, A., & Vergassola, M. (2000). Inverse energy cascade in two-dimensional turbulence: Deviations from Gaussian behavior. *Physics Review E*, *61*(1), R29–R32. https://doi.org/10.1103/physreve.61.r29

Boffetta, G., & Ecke, R. E. (2012). Two-dimensional turbulence. *Annual Review of Fluid Mechanics*, *44*(1), 427–451. https://doi.org/10.1146/annurev-fluid-120710-101240

Bryan, G. H., & Rotunno, R. (2009a). Evaluation of an analytical model for the maximum intensity of tropical cyclones. *Journal of the Atmospheric Sciences*, *66*(10), 3042–3060. https://doi.org/10.1175/2009JAS3038.1

Bryan, G. H., & Rotunno, R. (2009b). The maximum intensity of tropical cyclones in axisymmetric numerical model simulations. *Monthly Weather Review*, *137*(6), 1770–1789. https://doi.org/10.1175/2008MWR2709.1

Bryan, G. H., Rotunno, R., & Chen, Y. (2010). The effects of turbulence on hurricane intensity. In *29th conference on hurricanes and tropical meteorology, 8C.7*. American Meteorological Society.

Byrne, D., & Zhang, J. A. (2013). Height-dependent transition from 3-D to 2-D turbulence in the hurricane boundary layer. *Geophysical Research Letters*, *40*(8), 1439–1442. https://doi.org/10.1002/grl.50335

Cabanes, S., Gastine, T., & Fournier, A. (2024). Zonostrophic turbulence in the subsurface oceans of the Jovian and Saturnian moons. *Icarus*, *415*, 116047. https://doi.org/10.1016/j.icarus.2024.116047

Carr, L. E., & Elsberry, R. L. (1997). Models of tropical cyclone wind distribution and beta-effect propagation for application to tropical cyclone track forecasting. *Monthly Weather Review*, *125*, 3190–3209. https://doi.org/10.1175/1520-0493(1997)125⟨3190:MOTCWD⟩2.0.CO;2

Carr, L. E., & Williams, R. T. (1989). Barotropic vortex stability to perturbations from axisymmetry. *Journal of the Atmospheric Sciences*, *46*, 3177–3191. https://doi.org/10.1175/1520-0469(1989)046⟨3177:BVSTPF⟩2.0.CO;2

Chan, J. C.-L., & Williams, R. T. (1987). Analytical and numerical studies of the beta-effect in tropical cyclone motion. Part I: Zero mean flow. *Journal of the Atmospheric Sciences*, *44*(9), 1257–1265. https://doi.org/10.1175/1520-0469(1987)044<1257:aansot>2.0.co;2

Chaouche, L. Y., Cameron, R. H., Solanki, S. K., Riethmüller, T. L., Anusha, L. S., Witzke, V., et al. (2020). Power spectrum of turbulent convection in the solar photosphere. *Astronomy & Astrophysics*, *644*, A44. https://doi.org/10.1051/0004-6361/202037545

Charney, J. G. (1971). Geostrophic turbulence. *Journal of the Atmospheric Sciences*, *28*(6), 1087–1095. https://doi.org/10.1175/1520-0469(1971)028<1087:gt>2.0.co;2

Chavas, D. R., Lin, N., Dong, W., & Lin, Y. (2016). Observed tropical cyclone size revisited. *Journal of Climate*, *29*(8), 2923–2939. https://doi.org/10.1175/JCLI-D-15-0731.1

Chavas, D. R., Lin, N., & Emanuel, K. (2015). A model for the complete radial structure of the tropical cyclone wind field. Part I: Comparison with observed structure. *Journal of the Atmospheric Sciences*, *72*(9), 3647–3662. https://doi.org/10.1175/JAS-D-15-0014.1

Chavas, D. R., Reed, K. A., & Knaff, J. A. (2017). Physical understanding of the tropical cyclone wind-pressure relationship. *Nature Communications*, *8*(1), 1360. https://doi.org/10.1038/s41467-017-01546-9

Chekhlov, A., Orszag, S. A., Sukoriansky, S., Galperin, B., & Staroselsky, I. (1996). The effect of small-scale forcing on large-scale structures in two-dimensional flows. *Physica D*, *98*(2), 321–334. https://doi.org/10.1016/0167-2789(96)00102-9

Cohen, N., Galperin, B., & Sukoriansky, S. (2024). Zonons are solitons produced by Rossby wave ringing. *MDPI Atmosphere*, *15*(6), 711. https://doi.org/10.3390/atmos15060711

Corbosiero, K. L., Molinari, J., Aiyyer, A. R., & Black, M. L. (2006). The structure and evolution of Hurricane Elena (1985). Part II: Convective asymmetries and evidence for vortex Rossby waves. *Monthly Weather Review*, *134*(11), 3073–3091. https://doi.org/10.1175/MWR3250.1

Emanuel, K. (1995). Sensitivity of tropical cyclones to surface exchange coeffcients and a revised steady-state model incorporating eye dynamics. *Journal of the Atmospheric Sciences*, *52*(22), 3969–3976. https://doi.org/10.1175/1520-0469(1995)052<3969:sotcts>2.0.co;2

Emanuel, K., Velez-Pardo, M., & Cronin, T. W. (2023). The surprising roles of turbulence in tropical cyclone physics. *MDPI Atmosphere*, *14*(8), 1254. https://doi.org/10.3390/atmos14081254

Errico, R. M. (1985). Spectra computed from a limited area grid. *Monthly Weather Review*, *113*(9), 1554–1562. https://doi.org/10.1175/1520-0493(1985)113⟨1554:SCFALA⟩2.0.CO;2

Fiorino, M., & Elsberry, R. L. (1989). Some aspects of vortex structure in tropical cyclone motion. *Journal of the Atmospheric Sciences*, *46*, 979–990.

Franklin, J. L., Feuer, S. E., Kaplan, J., & Aberson, S. D. (1996). Tropical cyclone motion and surrounding flow relationships: Searching for beta gyres in Omega dropwindsonde datasets. *Monthly Weather Review*, *124*(1), 64–84. https://doi.org/10.1175/1520-0493(1996)124<0064:tcmasf>2.0.co;2

Frederiksen, J. S., & O'Kane, T. J. (2023). Realizable eddy damped Markovian anisotropic closure for turbulence and Rossby wave interactions. *MDPI Atmosphere*, *14*(7), 1098. https://doi.org/10.3390/atmos14071098

Frederiksen, J. S., & O'Kane, T. J. (2024). Turbulence and Rossby wave dynamics with realizable eddy damped Markovian anisotropic closure. *MDPI Fluids*, *9*(5), 116. https://doi.org/10.3390/fluids9050116

Galperin, B. & Read, P. L. (Eds.) (2019). *Zonal jets: Phenomenology, genesis, and physics*. Cambridge University Press. https://doi.org/10.1017/9781107358225.014

Galperin, B., & Sukoriansky, S. (2020). Quasinormal scale elimination theory of the anisotropic energy spectra of atmospheric and oceanic turbulence. *Physics Review Fluids*, *5*(6), 063803. https://doi.org/10.1103/PhysRevFluids.5.063803

Galperin, B., Sukoriansky, S., Dikovskaya, N., Read, P., Yamazaki, Y., & Wordsworth, R. (2006). Anisotropic turbulence and zonal jets in rotating flows with a β-effect. *Nonlinear Processes in Geophysics*, *13*(1), 83–98. https://doi.org/10.5194/npg-13-83-2006

Galperin, B., Sukoriansky, S., Young, R. M. B., Chemke, R., Kaspi, Y., Read, P. L., & Dikovskaya, N. (2019). Barotropic and zonostrophic turbulence. In B. Galperin & P. L. Read (Eds.), *Zonal jets: Phenomenology, genesis, and physics* (pp. 220–237). Cambridge University Press. https://doi.org/10.1017/9781107358225.014

Galperin, B., Young, R., Sukoriansky, S., Dikovskaya, N., Read, P., Lancaster, A., & Armstrong, D. (2014). Cassini observations reveal a regime of zonostrophic macroturbulence on Jupiter. *Icarus*, *229*, 295–320. https://doi.org/10.1016/j.icarus.2013.08.030

Gerber, E. P., & Thompson, D. W. J. (2017). What makes an annular mode "annular"? *Journal of the Atmospheric Sciences*, *74*(2), 317–332. https://doi.org/10.1175/JAS-D-16-0191.1

Golitsyn, G. S. (2018). Random Walk laws by A.N. Kolmogorov as the basics for understanding most phenomena of the nature. *Izvestiya Atmospheric and Oceanic Physics*, *54*(3), 223–228. https://doi.org/10.1134/s0001433818030064

Goncharov, V., & Pavlov, V. (2004). Null modes effect in Rossby wave model. *Nonlinear Processes in Geophysics*, *11*(3), 281–293. https://doi.org/10.5194/npg-11-281-2004

Green, B. W., & Zhang, F. (2015). Numerical simulations of Hurricane Katrina (2005) in the turbulent gray zone. *Journal of Advances in Modeling Earth Systems*, *7*(1), 142–161. https://doi.org/10.1002/2014MS000399

Guimond, S. R., Reasor, P. D., Heymsfield, G. M., & McLinden, M. M. (2020). The dynamics of vortex Rossby waves and secondary eyewall development in Hurricane Matthew (2016): New insights from radar measurements. *Journal of the Atmospheric Sciences*, *77*(7), 2349–2374. https://doi.org/10.1175/JAS-D-19-0284.1

Gunnarson, J. L., Sayanagi, K. M., Fischer, G., Barry, T., Wesley, A., Dyudina, U. A., et al. (2023). Multiple convective storms within a single cyclone on Saturn. *Icarus*, *389*, 115228. https://doi.org/10.1016/j.icarus.2022.115228

Holton, J. R. (2004). *An introduction to dynamic meteorology* (4th ed.). Elsevier Academic Press.

Huang, H.-P., Galperin, B., & Sukoriansky, S. (2001). Anisotropic spectra in two-dimensional turbulence on the surface of a rotating sphere. *Physics of Fluids*, *13*(1), 225–240. https://doi.org/10.1063/1.1327594

Irish, J. L., & Resio, D. T. (2010). A hydrodynamics-based surge scale for hurricanes. *Ocean Engineering*, *37*(1), 69–81. https://doi.org/10.1016/j.oceaneng.2009.07.012

Judt, F., Chen, S. S., & Berner, J. (2016). Predictability of tropical cyclone intensity: Scale-dependent forecast error growth in high-resolution stochastic kinetic-energy backscatter ensembles. *Quarterly Journal of the Royal Meteorological Society*, *142*(694), 43–57. https://doi.org/10.1002/qj.2626

Judt, F., Rios-Berrios, R., & Bryan, G. H. (2023). Marathon versus sprint: Two modes of tropical cyclone rapid intensification in a global convection-permitting simulation. *Monthly Weather Review*, *151*(10), 2683–2690. https://doi.org/10.1175/MWR-D-23-0038.1

Kantha, L. (2008). Tropical cyclone destructive potential by integrated kinetic energy. *Bulletin of the American Meteorological Society*, *89*, 219–221. https://doi.org/10.1175/BAMS-89-2-219

Kieu, C., & Rotunno, R. (2022). Characteristics of tropical-cyclone turbulence and intensity predictability. *Geophysical Research Letters*, *49*(8), e2021GL096544. https://doi.org/10.1029/2021GL096544

Knaff, J. A., Cram, T. A., Schumacher, A. B., Kossin, J. P., & DeMaria, M. (2008). Objective identification of annular hurricanes. *Weather and Forecasting*, *23*(1), 17–28. https://doi.org/10.1175/2007WAF2007031.1

Knaff, J. A., Kossin, J. P., & DeMaria, M. (2003). Annular hurricanes. *Weather and Forecasting*, *18*(2), 204–223. https://doi.org/10.1175/1520-0434(2003)018<0204:ah>2.0.co;2

Kolmogorov, A. N. (1934). Zufällige Bewegungen. *Annals of Mathematics*, *35*, 116–117.

Kuo, H.-C., Schubert, W. H., Tsai, C.-L., & Kuo, Y.-F. (2008). Vortex interactions and barotropic aspects of concentric eyewall formation. *Monthly Weather Review*, *136*(12), 5183–5198. https://doi.org/10.1175/2008MWR2378.1

Kurgansky, M. V. (2008). The energy spectrum in a barotropic atmosphere. *Advances in Geosciences*, *15*, 17–22. https://doi.org/10.5194/adgeo-15-17-2008

Landau, L. D., & Lifshitz, E. M. (1976). *Mechanics* (3rd ed.). Elsevier.

Lemasquerier, D., Favier, B., & Le Bars, M. (2023). Zonal jets experiments in the gas giants' zonostrophic regime. *Icarus*, *390*, 115292. https://doi.org/10.1016/j.icarus.2022.115292

Lorenz, E. N. (1963). Deterministic nonperiodic flow. *Journal of the Atmospheric Sciences*, *20*(2), 130–141. https://doi.org/10.1175/1520-0469(1963)020⟨0130:dnf⟩2.0.co;2

Lorenz, E. N. (1969). The predictability of a flow which possesses many scales of motion. *Tellus*, *21*(3), 289–307. https://doi.org/10.3402/tellusa.v21i3.10086

Lu, K.-Y., & Chavas, D. R. (2022). Tropical cyclone size is strongly limited by the Rhines scale: Experiments with a barotropic model. *Journal of the Atmospheric Sciences*, *79*(8), 2109–2124. https://doi.org/10.1175/JAS-D-21-0224.1

Macdonald, N. J. (1968). The evidence for the existence of Rossby-like waves in the hurricane vortex. *Tellus*, *20*(1), 138–150. https://doi.org/10.1111/j.2153-3490.1968.tb00358.x

Malkus, J. S., & Riehl, H. (1960). On the dynamics and energy transformations in steady-state hurricanes. *Tellus*, *12*, 1–20. https://doi.org/10.1111/j.2153-3490.1960.tb01279.x

Maltrud, M., & Vallis, G. (1991). Energy spectra and coherent structures in forced two-dimensional and β-plane turbulence. *Journal of Fluid Mechanics*, *228*, 321–342. https://doi.org/10.1017/s0022112091002720

21698996, 2025, 14, Downloaded from https://agupubs.onlinelibrary.wiley.com/doi/10.1029/2024JD042733, Wiley Online Library on [24/08/2025]. See the Terms and Conditions (https://onlinelibrary.wiley.com/terms-and-conditions) on Wiley Online Library for rules of use; OA articles are governed by the applicable Creative Commons License

Marenco, A., Thouret, V., Nédélec, P., Smith, H., Helten, M., Kley, D., et al. (1998). Measurements of ozone and water vapor by airbus in-service aircraft: The MOZAIC airborne program, an overview. *Journal of Geophysical Research*, *103*, 25631–25642. https://doi.org/10.1029/98JD00977

Martinez, J., Davis, C. A., & Bell, M. M. (2022). Eyewall asymmetries and their contributions to the intensification of an idealized tropical cyclone translating in uniform flow. *Journal of the Atmospheric Sciences*, *79*(9), 2471–2491. https://doi.org/10.1175/JAS-D-21-0302.1

McWilliams, J. C., Graves, L. P., & Montgomery, M. T. (2003). A formal theory for vortex Rossby waves and vortex evolution. *Geophysical & Astrophysical Fluid Dynamics*, *97*(4), 275–309. https://doi.org/10.1080/0309192031000108698

Möller, J. D., & Montgomery, M. T. (1999). Vortex Rossby waves and hurricane intensification in a barotropic model. *Journal of the Atmospheric Sciences*, *56*, 1674–1687. https://doi.org/10.1175/1520-0469(1999)056⟨1674:VRWAHI⟩2.0.CO;2

Monahan, A. H., & Fyfe, J. C. (2008). On annular modes and zonal jets. *Journal of Climate*, *21*(9), 1963–1978. https://doi.org/10.1175/2007JCLI1841.1

Monin, A. S., & Yaglom, A. M. (1975). *Statistical fluid mechanics*. MIT Press.

Montgomery, M. T., & Kallenbach, R. J. (1997). A theory for vortex Rossby waves and its application to spiral bands and intensity changes in hurricanes. *Quarterly Journal of the Royal Meteorological Society*, *123*(538), 435–465. https://doi.org/10.1002/qj.49712353810

Montgomery, M. T., Nicholls, M. E., Cram, T. A., & Saunders, A. B. (2006). A vortical hot tower route to tropical cyclogenesis. *Journal of the Atmospheric Sciences*, *63*(1), 355–386. https://doi.org/10.1175/jas3604.1

Montgomery, M. T., & Smith, R. K. (2017). Recent developments in the fluid dynamics of tropical cyclones. *Annual Review of Fluid Mechanics*, *49*(1), 541–574. https://doi.org/10.1146/annurev-fluid-010816-060022

Montgomery, M. T., Vladimirov, V. A., & Denissenko, P. V. (2002). An experimental study on hurricane mesovortices. *Journal of Fluid Mechanics*, *471*, 1–32. https://doi.org/10.1017/S0022112002001647

Murnane, R. J., & Elsner, J. B. (2012). Maximum wind speeds and US hurricane losses. *Geophysical Research Letters*, *39*(16), 707. https://doi.org/10.1029/2012GL052740

Nastrom, G. D., & Gage, K. S. (1985). A climatology of atmospheric wavenumber spectra of wind and temperature observed by commercial aircraft. *Journal of the Atmospheric Sciences*, *42*, 950–960. https://doi.org/10.1175/1520-0469(1985)042,0950:ACOAWS.2.0.CO;2

Nastrom, G. D., Gage, K. S., & Jasperson, W. H. (1984). Kinetic energy spectrum of large- and mesoscale atmospheric processes. *Nature*, *310*(5972), 36–38. https://doi.org/10.1038/310036a0

Nolan, D. S., & Montgomery, M. T. (2000). The algebraic growth of wavenumber one disturbances in hurricane-like vortices. *Journal of the Atmospheric Sciences*, *57*(21), 3514–3538. https://doi.org/10.1175/1520-0469(2000)057⟨3514:TAGOWO⟩2.0.CO;2

Nowak, J. L., Lothon, M., Lenschow, D. H., & Malinowski, S. P. (2025). The ratio of transverse to longitudinal turbulent velocity statistics for aircraft measurements. *Atmospheric Measurement Techniques*, *18*(1), 93–114. https://doi.org/10.5194/amt-18-93-2025

Oguejiofor, C. N., Bryan, G. H., Rotunno, R., Sullivan, P. P., & Richter, D. H. (2024). The role of turbulence in an intense tropical cyclone: Momentum diffusion, eddy viscosities, and mixing lengths. *Journal of the Atmospheric Sciences*, *81*(8), 1343–1369. https://doi.org/10.1175/JAS-D-23-0209.1

Ooyama, K. V. (1982). Conceptual evolution on the theory and modeling of the tropical cyclone. *Journal of the Meteorological Society of Japan*, *60*, 369–379.

Peng, J., Zhang, L., Luo, Y., & Zhang, Y. (2014). Mesoscale energy spectra of the Mei-Yu front system. Part I: Kinetic energy spectra. *Journal of the Atmospheric Sciences*, *71*(1), 37–55. https://doi.org/10.1175/JAS-D-13-085.1

Pope, S. B. (2018). *Turbulent flows* (4th ed.). Cambridge University Press.

Pouquet, A., Marino, R., Mininni, P., & Rosenberg, D. (2017). Dual constant-flux energy cascades to both large scales and small scales. *Physics of Fluids*, *29*(11), 111108. https://doi.org/10.1063/1.5000730

Prasanth, S., Chavas, D. R., Marks, F. D., Jr., Dubey, S., Shreevastava, A., & Krishnamurti, T. N. (2020). Characterizing the energetics of vortex-scale and sub-vortex-scale asymmetries during tropical cyclone rapid intensity changes. *Journal of the Atmospheric Sciences*, *77*(1), 315–336. https://doi.org/10.1175/JAS-D-19-0067.1

Read, P. L. (2024). The dynamics of Jupiter's and Saturn's weather layers: A synthesis after Cassini and Juno. *Annual Review of Fluid Mechanics*, *56*(1), 271–293. https://doi.org/10.1146/annurev-fluid-121021-040058

Riehl, H. (1963). Some relations between wind and thermal structure of steady state hurricanes. *Journal of the Atmospheric Sciences*, *20*(4), 276–287. https://doi.org/10.1175/1520-0469(1963)020<0276:srbwat>2.0.co;2

Rotunno, R., & Snyder, C. (2008). A generalization of Lorenz's model for the predictability of flows with many scales of motion. *Journal of the Atmospheric Sciences*, *65*(3), 1063–1076. https://doi.org/10.1175/2007jas2449.1

Sahoo, G., Alexakis, A., & Biferale, L. (2017). Discontinuous transitions from direct to inverse cascade in three-dimensional turbulence. *Physical Review Letters*, *118*(16), 164501. https://doi.org/10.1103/physrevlett.118.164501

Sánchez-Lavega, A., Orton, G. S., Hueso, R., García-Melendo, E., Pérez-Hoyos, S., Simon-Miller, A., et al. (2008). Depth of a strong jovian jet from a planetary-scale disturbance driven by storms. *Nature*, *451*(7177), 437–440. https://doi.org/10.1038/nature06533

Schecter, D. A. (2011). Evaluation of a reduced model for investigating hurricane formation from turbulence. *Quarterly Journal of the Royal Meteorological Society*, *137*(654), 155–178. https://doi.org/10.1002/qj.729

Shapiro, L. J., & Ooyama, K. V. (1990). Barotropic vortex evolution on a beta plane. *Journal of the Atmospheric Sciences*, *47*(2), 170–187. https://doi.org/10.1175/1520-0469(1990)047<0170:bveoab>2.0.co;2

Shen, W. (2006). Does the size of hurricane eye matter with its intensity? *Geophysical Research Letters*, *33*(18), L18813. https://doi.org/10.1029/2006GL027313

Smith, R. K., Montgomery, M. T., & Sang, N. V. (2009). Tropical cyclone spin-up revisited. *Quarterly Journal of the Royal Meteorological Society*, *135*, 1321–1335. https://doi.org/10.1002/qj.428

Stern, D. P., Vigh, J. L., Nolan, D. S., & Zhang, F. (2015). Revisiting the relationship between eyewall contraction and intensification. *Journal of the Atmospheric Sciences*, *72*(4), 1283–1306. https://doi.org/10.1175/jas-d-14-0261.1

Sukoriansky, S., Dikovskaya, N., & Galperin, B. (2007). On the 'arrest' of the inverse energy cascade and the Rhines scale. *Journal of the Atmospheric Sciences*, *64*(9), 3312–3327. https://doi.org/10.1175/jas4013.1

Sukoriansky, S., Dikovskaya, N., & Galperin, B. (2008). Nonlinear waves in zonostrophic turbulence. *Physical Review Letters*, *101*(17), 178501. https://doi.org/10.1103/physrevlett.101.178501

Sukoriansky, S., Dikovskaya, N., Grimshaw, R., & Galperin, B. (2012). Rossby waves and zonons in zonostrophic turbulence. In *AIP Conference Proceedings* (Vol. 1439, pp. 111–122). American Institute of Physics. https://doi.org/10.1063/1.3701355

Sukoriansky, S., & Galperin, B. (2016). QNSE theory of turbulence anisotropization and onset of the inverse energy cascade by solid body rotation. *Journal of Fluid Mechanics*, *805*, 384–421. https://doi.org/10.1017/jfm.2016.568

21698996, 2025, 14, Downloaded from https://agupubs.onlinelibrary.wiley.com/doi/10.1029/2024JD042733, Wiley Online Library on [24/08/2025]. See the Terms and Conditions (https://onlinelibrary.wiley.com/terms-and-conditions) on Wiley Online Library for rules of use; OA articles are governed by the applicable Creative Commons License

Tang, J. D., Byrne, D., Zhang, J. A., Wang, Y., t. Lei, X., Wu, D., et al. (2015). Horizontal transition of turbulent cascade in the near-surface layer of tropical cyclones. *Journal of the Atmospheric Sciences*, *72*(12), 4915–4925. https://doi.org/10.1175/JAS-D-14-0373.1

Thompson, P. D. (1973). The equilibrium energy spectrum of randomly forced two-dimensional turbulence. *Journal of the Atmospheric Sciences*, *30*(8), 1593–1598. https://doi.org/10.1175/1520-0469(1973)030⟨1593:TEESOR⟩2.0.CO;2

Trenberth, K. E., & Solomon, A. (1993). Implications of global atmospheric spatial spectra for processing and displaying data. *Journal of Climate*, *6*, 531–545. https://doi.org/10.1175/1520-0442(1993)006⟨0531:IOGASS⟩2.0.CO;2

Vinour, L., Jullien, S., Mouche, A., Combot, C., & Mangeas, M. (2021). Observations of tropical cyclone inner-core fine-scale structure, and its link to intensity variations. *Journal of the Atmospheric Sciences*, *78*(11), 3651–3671. https://doi.org/10.1175/JAS-D-20-0245.1

Vogelzang, J., Stoffelen, A., Verhoef, A., & Figa-Saldana, J. (2011). On the quality of high-resolution scatterometer winds. *Journal of Geophysical Research*, *116*(C10), C10033. https://doi.org/10.1029/2010JC006640

Vonich, P. T., & Hakim, G. J. (2018). Hurricane kinetic energy spectra from in situ aircraft observations. *Journal of the Atmospheric Sciences*, *75*(8), 2523–2532. https://doi.org/10.1175/JAS-D-17-0270.1

Wang, Y., & Wu, C.-C. (2004). Current understanding of tropical cyclone structure and intensity changes—A review. *Meteorology and Atmospheric Physics*, *87*(4), 257–278. https://doi.org/10.1007/s00703-003-0055-6

Wang, Y., Zhang, L., Peng, J., & Liu, S. (2018). Mesoscale horizontal kinetic energy spectra of a tropical cyclone. *Journal of the Atmospheric Sciences*, *75*(10), 3579–3596. https://doi.org/10.1175/JAS-D-17-0391.1

Wurman, J., & Kosiba, K. (2018). The role of small-scale vortices in enhancing surface winds and damage in Hurricane Harvey (2017). *Monthly Weather Review*, *146*(3), 713–721. https://doi.org/10.1175/MWR-D-17-0327.1

Yakhot, V., & Orszag, S. (1986). Renormalization group analysis of turbulence. I. Basic theory. *Journal of Scientific Computing*, *1*, 3–51. https://doi.org/10.1007/bf01061452

Yamagata, T. (1976). On trajectories of Rossby wave-packets released in a lateral shear flow. *Journal of the Oceanographical Society of Japan*, *32*(4), 162–168. https://doi.org/10.1007/bf02107270

Yu, S., Zhang, L., Wang, Y., & Peng, J. (2022). Mesoscale horizontal kinetic energy spectra of an eastward-moving southwest vortex. *MDPI - Atmosphere*, *13*(5), 653. https://doi.org/10.3390/atmos13050653

Zaqarashvili, T. V., Albekioni, M., Ballester, J. L., Bekki, Y., Biancofiore, L., Birch, A. C., et al. (2021). Rossby waves in astrophysics. *Space Science Reviews*, *217*(15), 1–93. https://doi.org/10.1007/s11214-021-00790-2

Zhai, A. R., & Jiang, J. H. (2014). Dependence of US hurricane economic loss on maximum wind speed and storm size. *Environmental Research Letters*, *9*(6), 064019. https://doi.org/10.1088/1748-9326/9/6/064019

Zhang, J. A. (2010). Spectral characteristics of turbulence in the hurricane boundary layer over the ocean between the outer rain bands. *Quarterly Journal of the Royal Meteorological Society*, *136*(649), 918–926. https://doi.org/10.1002/qj.610

Zhang, J. A., Black, P. G., French, J. R., & Drennan, W. M. (2008). First direct measurements of enthalpy flux in the hurricane boundary layer: The CBLAST results. *Geophysical Research Letters*, *35*(14), 210. https://doi.org/10.1029/2008GL034374

Zheng, H., Zhang, Y., Wang, Y., Zhang, L., Peng, J., Liu, S., & Li, A. (2020). Characteristics of atmospheric kinetic energy spectra during the intensification of typhoon Lekima (2019). *Applied Sciences*, *10*(17), 6029. https://doi.org/10.3390/app10176029

21698996, 2025, 14, Downloaded from https://agupubs.onlinelibrary.wiley.com/doi/10.1029/2024JD042733, Wiley Online Library on [24/08/2025]. See the Terms and Conditions (https://onlinelibrary.wiley.com/terms-and-conditions) on Wiley Online Library for rules of use; OA articles are governed by the applicable Creative Commons License